

A sample of low redshift BL Lacs. I. The radio data.

M. Giroletti and G. Giovannini

Istituto di Radioastronomia, via Gobetti 101, 40129, Bologna, Italy

Dipartimento di Astronomia, Università di Bologna, via Ranzani 1, 40127 Bologna, Italy

G. B. Taylor

National Radio Astronomy Observatory, P.O. Box O, Socorro, NM 87801, USA

and

R. Falomo

Osservatorio Astronomico di Padova, vicolo Osservatorio 5, Padova, Italy

ABSTRACT

We present a new sample of 30 nearby ($z < 0.2$) BL Lacs, selected to study the nuclear as well as the large scale properties of low power radio sources. In this first paper, we show and discuss new radio data taken with the VLA (19 objects at 1.4 GHz, either in A or C configuration, or both) as well as with the VLBA (15 sources at 5 GHz). On the kiloparsec scale, all objects exhibit a compact core and a variety of radio morphologies (jets, halos, secondary compact components). On the parsec scale, we find weak cores and a few short, one-sided, jets. From the jet/counter-jet ratio, core dominance, and synchrotron self Compton model we estimate the intrinsic orientation and velocity of the jets. The resulting properties of BL Lacs are similar to those of a parent population composed of FR I radio galaxies.

Subject headings: galaxies: active — galaxies: nuclei — galaxies: jets — BL Lacertae objects: general — radio continuum: galaxies

1. INTRODUCTION

Ever since the first suggestion of a possible unification of radio sources (e.g., Orr & Browne 1982), the viability for a comprehensive view of Active Galactic Nuclei (AGN) has been actively debated. A major achievement is the formulation of a scheme in which BL

Lac objects and quasars are the aligned counterparts of edge darkened (FR I) and edge brightened (FR II) radio galaxies, respectively (e.g., Urry & Padovani 1995). However, many important issues still need to be worked out. In particular, the class of BL Lac objects and its unification to FR I radio galaxies is an incessant source of puzzling questions.

For many years, when only a few objects were known, an apparent dichotomy was present within the BL Lac population. This dichotomy was based initially on selection criteria, separating X-ray and radio selected objects. Later on, the dichotomy was refined according to the position of the low energy peak in the spectral energy distribution (SED), with BL Lacs classified as either low (LBL) or high (HBL) frequency peaked objects. LBLs have the peaks of emitted energy (νF_ν) in the infrared/optical and MeV/GeV bands while HBLs peak at higher frequencies, namely UV/X-ray and GeV/TeV; furthermore, other observational differences between LBL and HBL have been found, including the fact that HBL have less dominant radio cores, a lower degree of optical polarization, and a possibly different cosmological evolution (see Rector et al. 2003, and references therein). However, multi-wavelength studies of larger samples seem to have solved this dichotomy, showing that the SED of BL Lacs (and emission line blazars) form a continuum, and that the emission peaks shift to higher frequency as the bolometric luminosity decreases (the so called *blazar sequence*, see Fossati et al. 1998). Donato et al. (2001) confirmed this trend considering more sources and hard X-ray data. Among possible explanations, Ghisellini et al. (1998) proposed that an increase in luminosity causes the emitting particles to suffer more severe radiative losses; in turn, this explains the shift of the peaks to lower frequency. There are however some problems with this scenario: following the discovery of a significant number of FSRQs with flat α_{RX} in a deep survey (the DXRBS, see Perlman et al. 1998; Landt et al. 2001), Padovani et al. (2003) considered a large sample of ~ 500 blazars, finding no evidence of anticorrelations between ν_{peak} and radio power (or other related quantities), as expected from the blazar sequence. Moreover, Caccianiga & Marchā (2004) present a few examples of low radio power BL Lacs with steep α_{RX} , suggesting that there may exist sources with a peak at low frequency and steep α_{RX} , as well as objects peaking at high frequency but still displaying flat α_{RX} (see also Anton et al. 2004).

In spite of our advances in understanding, most physical parameters remain difficult to determine in BL Lac objects. Several papers (see e.g. Falomo et al. 2002, and references therein) have addressed the long debated issue of determining the mass of the central black hole, finding values of order $10^8 - 10^9 M_\odot$. The situation remains more complicated for the jet physics and main parameters. On one hand, we have constraints from the detection of very energetic GeV and TeV photons, which require Doppler factor values $\delta > 10$ (Tavecchio et al. 1998); on the other hand, lower values are preferred from radio observations and from the lack of measured superluminal motions in most TeV sources (Giroletti et al. 2004; Piner

& Edwards 2004; Tingay & Edwards 2002). Even in sources where proper motions have been found (Homan et al. 2001; Jorstad et al. 2001), the estimated jet velocity from radio data is lower than the jet velocity required by high energy photons. This discrepancy suggests that the γ -rays and the radio photons may be produced in different regions of the jet, moving at different bulk velocities or differently oriented with respect to the line of sight. Furthermore, it is also possible that the jet has a dual *transverse* velocity or energetic structure; this may be needed to explain the different behaviour of optical cores in BL Lacs with respect to FR I radio galaxies (Chiaberge et al. 2000). In particular, the optical radiation could come from a faster spine, while the radio emission could originate in a slower, external layer of the jet. Evidence for a velocity structure in parsec scale jets has been found in some sources as 1144+35, Mkn 501, 3C 264, M87, 0331+39, 1055+018 (see e.g. Sol, Pelletier, & Asseo 1989; Hanasz & Sol 1996; Giovannini et al. 2001; Giroletti et al. 2004; Perlman et al. 1999, 2001; Attridge, Roberts, & Wardle 1999). The presence of a velocity structure could be due to the jet interaction with the interstellar medium (Giovannini et al. 2001) or could be an intrinsic jet property (Meier 2003).

As a matter of fact, the radio interferometry technique is an unique tool to determine parameters of the jet in the region from a few parsecs out to the kiloparsec scale structure, by means of studying observational properties such as jet sidedness, core dominance, and proper motion of knots (Giovannini 2003). Very Long Baseline Interferometry (VLBI) studies have yielded significant results for a number of sources, including a possible signature of the double velocity structure in the limb brightened jet of Markarian 501 (Giroletti et al. 2004). However, systematic and detailed VLBI studies on sizeable samples of BL Lacs are mostly based on bright, flux-limited catalogues, such as the 1 Jy sample (Stickel et al. 1991). By its very definition, this sample consists mostly of powerful and distant objects. These bright sources have yielded some interesting results, among which is a high incidence of FR II structures in the parent population (Rector & Stocke 2001; Cassaro et al. 1999). Moreover, objects in this sample present often a significant bending between parsec and kiloparsec scale structure (Cassaro et al. 2002), resulting in a peculiar bimodal distribution of the misalignment angle between the structure on the two scales (see also Appl et al. 1996, and references therein).

As for the weaker objects, parsec scale studies similar to those discussed above are still missing or based on small numbers of objects (Rector et al. 2003; Kollgaard et al. 1996). Given the SED shape for BL Lacs, objects weak in the radio are usually classified as HBL. Thus far, almost all BL Lacs detected at TeV energies belong to this sub-class. Moreover, weak objects are more easily found at low redshift, so that the high angular resolution of VLBI techniques allows observers to investigate the very innermost regions (1 mas \sim 2 pc

at $z = 0.1$)¹.

In order to investigate the above issues and to extend the current view to the low- z objects, we concentrated our attention on the sample of Falomo et al. (2000), who studied the host galaxies of 30 low redshift ($z < 0.2$) BL Lacs with the *Hubble Space Telescope* (HST). We carried out new radio observations of this sample, to look for differences in morphology with more powerful objects and to derive parameters for jet physics. In this paper, we present the new observations, and summarize data from the literature. By using all available data we can study the intrinsic power and parent population. In a forthcoming paper (Giroletti et al. in prep.), we will focus on the radio/optical comparison.

The sample selection is illustrated in §2, along with the main results of Falomo et al. (2000). Our observations are described in §3; we present the results in §4 and discuss them in §5. Finally, §6 summarizes the main results.

2. THE SAMPLE

2.1. Sample selection

By merging 7 flux limited samples², Scarpa et al. (2000) have collected a total of 132 BL Lac objects. The HST snapshot image survey of BL Lacs (Urry et al. 2000; Scarpa et al. 2000) has provided a homogeneous set of short-exposure, high-resolution images through the F702W filter for 110 objects in the sample. From this large dataset, Falomo et al. (2000) extracted a sub-sample of 30 low redshift ($z < 0.2$) objects for which it was possible to perform a detailed study of the properties of the host galaxy.

We now discard three objects from this sample: 1853+671 and 2326+174, which have a redshift slightly larger than 0.2 ($z = 0.212$ and 0.213 , respectively), and 2005–489, which is too far south to be observed with comparable quality high resolution imaging. Conversely, we add three more objects, which also have $z < 0.2$ and high quality HST observations available. The objects are 1215+303 ($z = 0.130$, Perlman et al. private communication), 2254+074 ($z = 0.190$), and 1652+398 (Mkn 501, $z = 0.034$). In total we have 30 objects. Although the sample cannot be considered complete, the selection process appears free from

¹Throughout this paper, we assume $H_0 = 71 \text{ km s}^{-1} \text{ Mpc}^{-1}$ and $q_0 = 0.5$.

²The 7 samples are: 1 Jy (Stickel et al. 1991); S4 (Stickel & Kuehr 1994); PG (Green et al. 1986); HEAO-A2 (Piccinotti et al. 1982); HEAO-A3 (Remillard et al. 1999); EMSS (Morris et al. 1991; Stocke et al. 1991; Rector et al. 2000); Slew (Schachter et al. 1993; Perlman et al. 1996)

significant biases with respect to source orientation and jet velocity.

Table 1 presents the full list of objects in the sample³. HBLs are clearly dominant, and most objects have been originally selected at X-ray energies. This selection is significantly different from most previous studies at radio frequencies. We note that HBLs have lower total luminosities and are particularly weak in the radio. Figure 1 plots, as histograms, the distribution of total power at 1.4 GHz for objects in the present sample compared to the 1 Jy sample. The two distributions are significantly different with $\langle \text{Log}P_{1.4\text{GHz}} \rangle = 24.7 \pm 0.6 \text{ W Hz}^{-1}$ and $26.7 \pm 0.9 \text{ W Hz}^{-1}$, respectively (some objects in the 1 Jy sample lack redshift information and were not considered). This is largely due to the large flux limit of the 1 Jy sample; furthermore, with no cut in redshift, it contains a number of high- z BL Lacs that bias the sample toward more powerful objects.

However, we note that there is some overlap between the two populations. Six of the objects belong to both samples (1418+546, 1514–241, 1652+398, 1807+698, 2200+420, 2254+074); indeed, these are well known objects, such as BL Lac itself, Mkn 501, and 3C 371. In contrast, most of the weakest HBL lack radio images on the parsec and/or kiloparsec scale.

2.2. Host Galaxies: a Summary

For these low- z objects it was possible with HST to investigate features and structures in the host galaxy that are undetectable with ground-based observations (Falomo et al. 2000). The host galaxy can be investigated within less than 1 kpc from the nucleus (corresponding to 0''.3 at $z = 0.2$). In particular one can search for slight offsets of the nucleus with respect to the galaxy center, determine the presence of sub-components in the host galaxy, investigate the detailed shape of the isophotes, and search for dust features and close companions.

The detailed analysis of HST images indicates that, in spite of the presence of the active nucleus, the host galaxy appears in most cases to be a completely “normal” elliptical. Both the ellipticity and the isophotal shape distributions are similar to those for radio galaxies and radio-quiet ellipticals. This suggests that tidal interactions are very infrequent or are short-lived with respect to the nuclear activity time scale.

There are no indications of displacements and/or off-centering of the galaxy isophotes

³The optical spectra of 0521–365 (Scarpa, Falomo, & Pian 1995) and 2201+044 (Veron-Cetty & Veron 1993; Falomo, Scarpa, & Bersanelli 1994) show emission and absorption lines and are similar to Seyfert 1 spectra but with lines of lower luminosity. At HST resolution the optical sources are fully resolved into nucleus, host galaxy, and a jet that contains some structures.

with respect to the nucleus, meaning the unresolved nuclear source truly sits in the center of the galaxy. This rules out the microlensing hypothesis for BL Lacs, which predicts frequent offsets for the nucleus with respect to the host galaxy.

The HST images have consistently shown that BL Lac hosts are virtually all massive ellipticals (average luminosity $M_R = -23.7 \pm 0.6$ and effective radius $R_e = 10$ kpc) typically located in poor groups. Moreover, these data have shown that no significant difference is present between the hosts of HBL and those of LBL in spite of the remarkable differences in their SED (Urry et al. 2000).

3. OBSERVATIONS AND DATA REDUCTION

Observations were aimed at completing the imaging for all the sources in the sample, both on arcsecond (Table 2) and milliarcsecond (Table 3) scales. We present the final images in Fig. 2–6 (see Tab. 4 for image parameters). Objects with good images available in the literature were not re-observed; see Table 5 for a summary of references.

3.1. VLA observations

We obtained observations with the NRAO⁴ Very Large Array (VLA) at 1.4 GHz on 2002 February 22 and May 3 in A configuration and on 2002 October 8 in C configuration (see Table 2 for a summary of the observations). In order to optimize the (u, v) coverage we observed in snapshot mode with two or three scans per source at different hour angles. On average, each source was observed for about 16 minutes after allowing for observations of calibrators and slewing of the telescope. We used the NRAO Astronomical Image Processing System (AIPS) to reduce the data and perform imaging with the standard phase self-calibration technique. Amplitude self-calibration was used only for the strongest sources (> 100 mJy) to obtain a better dynamic range. For fainter sources, amplitude self calibration is not necessary since images are noise limited and not dynamic range limited; moreover, spurious solutions could be introduced because of the low signal to noise ratio. We produced images with different weight distribution (uniform and natural) and did not find significative differences. Images presented here have been obtained with a weight in between the natural and uniform (ROBUST 0 in the task IMAGR in AIPS). This weighting scheme yields a typical

⁴The National Radio Astronomy Observatory is operated by Associated Universities, Inc., under cooperative agreement with the National Science Foundation.

final restoring beam of $\sim 1.9'' \times 1.2''$ for A configuration and of $\sim 15'' \times 11''$ for C configuration data; the average noise is $\sim 70 \mu\text{Jy}/\text{beam}$ and $\sim 140 \mu\text{Jy}/\text{beam}$, respectively. Images of sources in the southern hemisphere have more elliptical beams and slightly higher noise.

In total, we imaged 19 objects with the array in A configuration and 9 in C configuration. For the eight sources observed with both arrays, we combined the two final self-calibrated data-set using AIPS task `DBCON`. This yields better sensitivity (about a factor $\sqrt{2}$) and intermediate resolution. However, the (u, v) -coverage is not optimal, and the process of self-calibration can fail to converge, especially when extended flux detected in C configuration is over-resolved by the A array. For this reason, we only present combined array images for five sources (0145+138, 0229+200, 0347–121, 1959+650, and 2356–309).

3.2. VLBA observations

Very Long Baseline Interferometry observations have been performed with the NRAO Very Long Baseline Array (VLBA) for 15 sources on 2002 February 17, 18, and 19, at a frequency of 5 GHz (see Table 3 for a summary of the observations). A single VLA antenna was substituted for the VLBA antenna at Pie Town. We recorded 4 IFs (at 4971.49, 4979.49, 4987.49, 4995.49 MHz) with 8 MHz bandwidth each, in full polarizations. The data were correlated in Socorro and the reduction was performed in AIPS. All data were globally fringe fitted (Schwab & Cotton 1983) and then self calibrated. However, the VLA observations in A configuration provided us with new and precise position measurements. Since we had good positions for our target sources, we were able to avoid fringe-fitting the data for weak sources, which easily fails. Amplitude calibration was initially done using the standard method of measuring system temperatures and antenna gains calibration, followed by gain refinement using strong point-like calibrators.

On average, we have 45 minutes of useful data for each source, providing a nominal thermal noise of $\sim 0.11 \text{ mJy beam}^{-1}$. All our images have noise figures within a factor 2 from this. All sources are detected above the 3σ level, even the weakest. For 6 sources, only a faint point-like component was detected. For the remaining 9 strongest sources, we imported the (u, v) data into DIFMAP (Shepherd, Pearson, & Taylor 1994, 1995) for further self-calibration and imaging.

4. RESULTS

4.1. arcsec scale

We present our final images in Fig. 2–5 (see Tab. 4 for image parameters) and a list of flux densities for all objects in Tab. 5. We also include low frequency (325 MHz) data (Column 4), as measured in the Westerbork Northern Sky Survey (WENSS, Rengelink et al. 1997) or from the Texas Survey (Douglas et al. 1996). For sources lacking flux density measurement from both surveys, we estimate the flux density from the 1.4 GHz NRAO VLA Sky Survey (NVSS, Condon et al. 1998) assuming the average spectral index obtained from other sources, i.e. $\alpha = 0.11$. This is a sensible choice as all values obtained are below the sensitivity threshold (or out of the sky coverage) of both surveys. For 0521–365 only, whose radio data is missing because of its location, we interpolate the large number of measured fluxes available in the literature from 80 MHz to 8800 MHz. Columns 5 and 6 give the total and core flux densities at 1.4 GHz, and Column 7 lists the ratio between these values. We also report the core flux density at 5 GHz in Col. 8 and the corresponding reference in Col. 9. Finally, in Col. 10 we classify sources according to their arcsecond scale morphology.

For the sake of homogeneity, the total flux densities at 1.4 GHz (Col. 5) are all measured on data from the NVSS. We used, however, information from our higher resolution observations in order to separate possible contribution from confusing sources: the A array images show that this is needed only in 0145+138, in which we subtracted 8 mJy from the NVSS total. For objects observed also in C configuration, we consider the total flux density measured on our images as well and find that the deviation from the NVSS datum is always within $\pm 10\%$; such a small difference in the total flux density does not affect our results and it is probably due to core variability effects. In any case, there are no indications that the NVSS systematically overestimates the total flux density. The core value (Col. 6) has been measured using JMFIT in AIPS on our A configuration images (or from the literature, as given in the notes); the corresponding ratio between core and total flux is listed in Col. 9. In general, the core is the strongest component and accounts for most of the flux. In two objects (1418+546 and 1514–241), the core flux density is even larger than the total; this is probably due to variability of the core. At the other extreme, there are a number of sources (10/30) where a significant fraction of flux ($> 50\%$) is found in extended regions or in secondary components.

We find 9 sources where the core is the dominant component; 8 objects with a core-jet morphology; 4 with a core-halo morphology; 7 objects with more than one compact component – possibly a hot spot or a background source; and 2 objects (0548–322 and 0829+047) which are located in rich clusters and are clearly wide-angle-tail (WAT) radio

sources.

The objects span a range in total power of about 2.5 orders of magnitude at 1.4 GHz. The weakest object is 1255+244, which has $\text{Log}P_t = 23.88 \text{ W Hz}^{-1}$, whilst the most powerful is 0521–365, with $\text{Log}P_t = 26.07 \text{ W Hz}^{-1}$.

4.2. milliarcsecond structure

On VLBI scales, our 5 GHz observations have a typical resolution of $\sim 3.8 \text{ mas} \times 1.5 \text{ mas}$ and noise level of a few 0.1 mJy/beam. Figure 6 presents the images; Table 6 summarizes the most significant parameters: peak flux densities, total intensity, presence of a jet, and jet position angle (PA).

All objects are dominated by a strong, compact component. In five sources this component is responsible for all the correlated flux density and in two cases (0548–322 and 1440+122) there is little ($\sim 10\%$) flux density in extended structures that we could not image. Short one-sided jets (typically $< 10 \text{ mas}$) are present in seven sources and only 0521–365 presents a longer jet; in any case, the core is always the strongest component. No counter-jet is detected in any of the sources.

We have modelfitted the visibilities of all the sources in Difmap. In most cases, we need only one component (in addition to the core) to describe the jet. When two or more components are required, they usually align on a straight path, without showing significant bending. However, a comparison to the largest scale structure indicates that some bending occurs at large distance from the core.

Finally, from our model-fit we determine the jet brightness B_j and the jet/counter-jet ratio R_{\min} , which are presented in Columns 7 and 9 of Table 6. Since no object in the sample has a detectable counter-jet, the values presented are only lower limits based on the noise of the images. This is also true for objects with values derived from literature data (see notes to Table 6).

4.3. Parsec/Kiloparsec Scale Comparisons

A comparison of the morphology on parsec and kiloparsec scales reveals in general a good agreement, and objects in the present sample do not exhibit large bending between small and large scales. There are 10 sources that bend $\leq 30^\circ$, two between 30° and 60° , and two more are $> 60^\circ$; for the others there is no preferred direction on either parsec or

kiloparsec scale. Even with this uncertainty, this result seems to support the view proposed by Rector et al. (2003), i.e. that HBLs tend to have less bent jets than LBLs (see Fig. 7 and next section for discussion). It is also worth noting that all three objects showing an optical and X-ray jet (0521–365, 1807+698, and 2201+044, all LBLs), present straight jets as well. Therefore, with few exceptions, it seems that large bending in BL Lacs is not common; this agrees with the expectations of unified models, given the findings of Giovannini et al. (2001) that FR I radio galaxies show a good agreement between parsec and kiloparsec scale jet PA. Large bending in the jets is also unlikely in those objects presenting a core+halo morphology, such as 1133+704, 1215+303 (see FIRST image, Becker, White, & Helfand 1995), 1426+428, 1807+698, and 2344+514. The classic explanation is that the halos are lobes seen end on, and the main axis of the object is closely aligned with the line-of-sight. This explanation argues against large bends in the jet in these sources as well.

In the comparison between the arcsecond core at 5 GHz and the correlated VLBI flux at the same frequency (given in Tab. 5 and 6, respectively) there is a continuity of behavior – only 9 sources have integrated VLBI flux densities $\leq 60\%$ of their arcsecond core flux density. This result suggests that only a small fraction ($\sim 30\%$) of BL Lacs objects have a complex sub-arcsecond structure not visible in our data. In the majority we can follow the structure from parsec to kiloparsec scales.

Observational data suggest that beaming effects play a major role on the parsec scale and become less important on larger (kpc) scales. One clear piece of evidence is the presence of the symmetric structure on the kiloparsec scale in sources with an asymmetric parsec scale morphology. In sources discussed here we have 5 sources where VLA images suggest/show the presence of symmetric structure. They are: 0229+200, 0706+591, 0829+046, 1807+698, and 1959+650. These results imply that at a projected distance of 5-10 kpc from the core the jet velocity is no longer relativistic. On the contrary, some sources are still asymmetric in the VLA images. They are: 0145+138, 0347–121, 0927+500, and 1212+078. Assuming intrinsically symmetric jets and Doppler favoritism as the origin of observed asymmetries, the radio jets of these sources are still relativistic on scales of tens of kpc.

4.4. Notes on individual sources

0145+138 – This is one of the weakest objects ($\log P_{\text{tot}, 1.4\text{GHz}} = 24.19 \text{ W Hz}^{-1}$), to show a core-jet structure. The jet is unusually long for such a low-power object, as it extends for ~ 200 kpc eastward. On the opposite side of the core, $\sim 25''$ westward, there is a secondary component, which is associated with an elliptical galaxy with the same redshift, as previously noted by Perlman et al. (1996) (see also Slinglend et al. 1998); our A array image resolves

this source into a double. Other nearby sources are possibly related to the foreground galaxy cluster Abell 257. Note that the total flux given in Tab. 5 refers to the BL Lac source only; the contribution of the nearby source has been subtracted. The VLBA image shows only a 3 mJy core in agreement with the core flux density from the VLA in A configuration. We surmise that most of the flux density in this source is from the long, one-sided jet.

0229+200 – The C-array image suggests, and the A+C image confirms, the presence of a two-sided jet, with the main jet pointing to the south, in agreement with Rector et al. (2003). About 100" to the north, we find a compact radio source not yet identified optically. The flux density of the VLBI core is ~ 16 mJy; no jet is visible on the parsec scale. Thanks to a longer exposure and better (u, v) -coverage, the VLBA image by Rector et al. (2003) shows a parsec scale jet, well aligned with the kpc scale main jet.

0347–121 – This object shows in the A array image a jet in PA -12° ; at 7" from the core the jet bends by $\sim 35^\circ$ and expands with a large opening angle, showing in the A+C image a lobe-like structure. The VLBI image gives no indication of a parsec scale jet.

0350–371 – Because of its low declination (Dec = -37°), this object has a somewhat lower resolution A configuration image. There is an indication of a jet present both on arcsec and milliarcsec scales, as an elongation of the main component to the north-east in PA 33° and 46° , respectively. This yields a small bend of $\Delta\text{PA} \sim -13^\circ$ from the parsec to the kiloparsec scale.

0521–365 – This is a nearby ($z = 0.055$), bright EGRET source (Lin et al. 1995). The optical spectrum of this objects exhibits prominent and variable emission lines (Scarpa, Falomo, & Pian 1995) and it was also classified as N galaxy and Seyfert galaxy, although its host galaxy is a luminous giant elliptical (Falomo 1994). This source is also well known for the presence of a prominent radio and optical jet (Danziger et al. 1979; Keel 1986; Falomo 1994), which resembles that of the nearby radio galaxy M87 (i.e. Sparks, Biretta, & Macchetto 1994). The optical jet is well aligned with the kiloparsec radio jet, and the radio and optical structures have a clear correspondence (Scarpa et al. 1999). Our VLBA image shows that the same PA found on the parsec scale jet is maintained, without any significant bending, over three orders of magnitude. This is consistent with a relatively large angle of view, in agreement with the absence of superluminal motion showed by Tingay & Edwards (2002) and the findings of Pian et al. (1996).

0548–322 – This southern object resides in a rich environment, with close companions and other galaxies at the same redshift (Falomo et al. 1995). This is in agreement with the wide-angle tail (WAT) structure revealed on kiloparsec scales by Laurent-Muehleisen et al. (1993) and Reid et al. (1999). The parsec scale image is dominated by a 35 mJy core,

with little or no other emission detected. The large difference between this value and the kiloparsec total flux density suggests that the emission on large scales is spread over an extended low brightness area.

0706+591 – Our image in A configuration is a significant improvement in resolution with respect to the only image published so far (Laurent-Muehleisen et al. 1993). The main structure is quite extended, broad, and the core is located at the north-west edge of this quite round cocoon. It could be a tailed radio structure (WAT or NAT) viewed at a small angle of sight. Note however that there is no indication of an overdensity of galaxies in its vicinity. A small orientation angle is also suggested by the different direction of the parsec scale core-jet structure ($\Delta\text{PA} \sim 80^\circ$).

0806+524 – This source is heavily core-dominated. It looks point-like with the VLA, with a flux density of 160 mJy/beam at 1.4 GHz. On the VLBI scale, the integrated flux density at 5 GHz is 137 mJy, distributed in a core and a short (~ 5 mas), northbound ($\text{PA} \sim 13^\circ$) jet.

0829+046 – This is one of the rare BL Lacs in which there is evidence of emission on both sides of the core. In the VLA A array image, two symmetric jets emerge at $\text{PA} 110^\circ$ (and -70°). Both jets bend, showing a radio structure typical of head-tail radio galaxies. For this reason, we believe that the large bending of the jet is related to this motion and not intrinsic to the source (see also Antonucci & Ulvestad 1985). This leaves us with a bend between parsec and kiloparsec scale of 44° (see VLBA image in Jorstad et al. 2001; Fey & Charlot 2000; Lister, Marscher, & Gear 1998).

0927+500 – This is the second most distant source in the sample and looks like a faint (~ 20 mJy), core-dominated source. No information is available on the parsec scale morphology.

1133+704 – Our observation reveals a core-halo morphology, confirming the claim of Wardle et al. (1984). The halo is faint and heavily resolved in the image in A configuration. This explains the results of Laurent-Muehleisen et al. (1993): in their 5 GHz image, the halo is resolved out and only the compact 125 mJy core is detected. The major axis of the halo is in the east-west direction, i.e. well aligned with the parsec scale jet detected by Kollgaard et al. (1996).

1212+078 – This object presents a good alignment between the parsec and kiloparsec scale structure. The jet is oriented at $\sim 90^\circ$ and is detected for 12 mas with the VLBA and almost 50" with the VLA. Rector et al. (2003) present a VLBA image (1997 May 17) and a deep B array VLA image suggesting a transverse orientation for the extended structure. A compact feature 40 mas south of the core is present in our image as well as in the one of

Rector et al. (2003). It is likely that our VLA image resolves some of the extended emission, which is also visible in Perlman et al. (1996) on the opposite side, as well as in the FIRST and NVSS images.

1218+304 – We confirm that this source is compact on kiloparsec scales (see Perlman 1994; Laurent-Muehleisen et al. 1993, and references therein) and place an upper limit on its size of $0.19''$; at the redshift of 1218+304 ($z = 0.182$, Perlman et al., private communication), this corresponds to 0.7 kpc. The VLBA image reveals a 10 mas jet emerging at $\text{PA} \sim 90^\circ$. The total VLBA correlated flux is 57 mJy and dominates the total flux density of the source.

1229+643 – The kiloparsec scale structure shows an almost unresolved core (see also Perlman 1994), with a little emission from a halo-like feature. However, even if the poor signal-to-noise of this structure does not allow us to make any strong claim about its nature, we can estimate that it is oriented at a PA of $\sim -20^\circ$. This is in general agreement with the previous image from Perlman & Stocke (1993). The VLBA jet points in direction northwest ($\text{PA} = -43^\circ$) and the core-jet structure accounts for most of the flux density from this source. Therefore, we tentatively propose a $\Delta\text{PA} \lesssim 25^\circ$.

1255+244 – This extremely weak object is only marginally resolved with the VLA, and barely detected by the VLBA (~ 3 mJy core). This is the weakest object in the sample ($\text{Log}P_{\text{tot},1.4\text{GHz}} = 23.5 \text{ W Hz}^{-1}$)

1426+428 – The comparison of the NVSS total flux density (61 mJy) and the peak of the A array image (32 mJy/beam) indicates that some extended emission is present. Our image confirms the presence of a faint halo surrounding the central core, but does not recover all the flux. Since previous images in C array (Laurent-Muehleisen et al. 1993) detected an intermediate value of 46 mJy, we believe that the difference has to be ascribed to resolution effects rather than variability. The NW extension is oriented at $\text{PA} \sim 50^\circ$ and therefore presents a $\Delta\text{PA} = 30^\circ$ with respect to the inner structure studied by Kollgaard et al. (1996). Note that this is a TeV source (Aharonian et al. 2002; Horan et al. 2002).

1440+122 – Little information can be obtained for this object. The VLBA image reveals only a faint (15 mJy) core, possibly extended to the west. VLA images obtained by Giovannini et al. (2004) show a nuclear flat spectrum nuclear emission surrounded by a steep spectrum halo structure $\sim 8''$ in size at 8.4 GHz moderately elongated in the SW direction.

1728+502 – The 200 mJy core dominates the source; it is slightly resolved to the northwest in the A configuration image. The C array VLA image detects ~ 16 mJy of extended emission in the same direction (in $\text{PA} -30^\circ$), spread over more than $100''$. A bending of $\sim 25^\circ$ west is required from the parsec scale jet shown by VLBA (Kollgaard et al. 1996) and EVN+MERLIN images (Giroletti et al., in preparation).

1807+698 – This is a well known source (3C 371), with a jet detected in the optical with the HST (Scarpa et al. 1999) and in the X-rays with *Chandra* (Pesce et al. 2001). This jet does not bend significantly and is well aligned (in PA $\sim 100^\circ$) with the parsec scale jet imaged with the Space VLBI by Gómez & Marscher (2000). The orientation is in good agreement with the PA of the jet visible in our C array image (ΔPA consistent with 0) and of the main lobe detected in the deep B array image at 5 GHz by Wrobel & Lind (1990); see also the 5 GHz and 15 GHz VLA observations of O’Dea, Barvainis, & Challis (1988). Thanks to the lower frequency and more compact configuration, we also detect a diffuse halo of about 340 mJy, surrounding both lobes and extending over 200"(see also Cassaro et al. 1999).

1959+650 – Costamante & Ghisellini (2002) suggested that this object could be a TeV source; in fact, a strong detection of very high energy γ -rays was obtained with the Whipple 10 m telescope (Holder et al. 2003) and the HEGRA Cherenkov telescopes (Aharonian et al. 2003), confirming the preliminary result presented by Nishiyama et al. (2000). Our C array radio image clearly shows a peculiar two-sided structure. The combination of A and C data indicates that the symmetry could be in the jet region, suggesting that the source is oriented in the plane of the sky and/or that the jet is non-relativistic on the arcsecond scale. The parsec scale jet in the image by Rector et al. (2003) at 5 GHz has a PA of -5° indicating that the jet does not change direction over three orders of magnitude. Note, however, that high frequency (15 GHz) observations suggest a 1 mas jet to the southeast, in PA $\sim 160^\circ$ (Piner & Edwards 2004).

2254+074 – This source has one of the brightest cores ($\text{Log}P_{\text{c},5\text{GHz}} = 26.1 \text{ W Hz}^{-1}$). Only a little extended emission is present on arcsecond scale, both in the A and C configuration. A comparison to the parsec scale total flux density (350 mJy, Fey & Charlot 2000), indicates that some emission originates on intermediate scales.

2344+514 – This is one of the most puzzling sources in the sample. VLA images show two bright components within 200" (180 kpc) from the position of the optical and radio core. Furthermore, extended, low-brightness emission is present between the core and the eastern feature. The A array observation resolves the faint emission, revealing a core-halo morphology, while the eastern feature appears extended in the direction of the core. Since this extension is visible also in the C array image (as well as in the B array map of Rector et al. 2003), it cannot be ascribed to bandwidth smearing. This elongation and the diffuse radio bridge connecting it to the core indicates that the component is related to the source. On the contrary, the NW component does not show any radio structure suggesting a connection. Finally, the VLBA image shows a jet oriented at 142° (see also Rector et al. 2003), confirming the complexity of this source ($\Delta\text{PA} \sim 45^\circ$ to the VLA main axis). Notice also that Catanese

et al. (1998) report a TeV detection from this source and that *Chandra* observations reveal diffuse X-ray emission in its environment (Donato et al. 2003).

2356–309 – Two components separated by 36" are connected by a weaker “bridge”, resolved by the VLA in A configuration. A third component is found on the opposite side. The core is barely detected on the parsec scale, due to the low declination (-30°) and flux density (21 mJy) of this BL Lac. Because of the presence of a core, a radio bridge, and two possibly related compact structures, this source is similar to 2344+514.

5. DISCUSSION

According to the current view of the unification of AGNs, BL Lac objects are expected to be FR I radio galaxies oriented at a small angle with respect to the line-of-sight. Moreover, radio data (e.g., Giovannini et al. 2001) as well as variability, one sidedness, superluminal motion and high frequency emission (X- and γ - rays) strongly support the existence of relativistic jets. In agreement with the presence of fast jets and small angles to the line of sight, BL Lacs are usually core-dominated objects. However, we note that in our sample we have 10/30 objects where the core flux density is $< 50\%$ of the total flux density at 1.4 GHz.

Under the standard assumption that jets are intrinsically symmetric, we can derive constraints on the jet velocity and orientation. The approaching jet is amplified by relativistic beaming and the counter-jet is de-boosted. The observed ratio R between the observed jet and counter-jet brightness is related to the intrinsic jet velocity β and orientation angle θ by $R = \left(\frac{1 + \beta \cos \theta}{1 - \beta \cos \theta} \right)^p$, where $p = 2 + \alpha$ (continuous jet) or $p = 3 + \alpha$ (moving sphere). Here we assume a continuous jet, with spectral index $\alpha = 0.5$ ($S(\nu) \propto \nu^{-\alpha}$), following Giovannini et al. (1994) and references therein.

However, in BL Lacs the counter-jet is generally de-boosted below the detection threshold on the parsec scale and we can only determine lower limits R_{\min} . Furthermore, since our sample is dominated by faint objects, the main jet shows in most cases a low brightness emission resulting in a small R_{\min} . Therefore, in most cases we do not find significant constraints on β and θ ; only in 6 objects the J/CJ ratio is $R_{\min} > 100$. In these cases, we give the relative limits on $\beta \cos \theta$ in Table 6 (Col. 10).

The relativistic boosting at the base of the jet affects the observed radio power of the core; by comparing this value to that expected from the total power at low frequency via the correlation found by Giovannini et al. (1988, 2001), we can derive the amount of boosting. We account for variability, which results in a range of possible Doppler factors for each source

after allowing for a variation of a factor 2 in the core flux density. Considering these intervals, we estimate for each object the allowed orientation angle under the assumption of a Lorentz factor $\Gamma = 5$. We note that larger Lorentz factors do not change significantly the permitted angles, while values $\Gamma < 3$ are not allowed, according to Giovannini et al. (2001) and from strong and widely accepted lines of evidence (superluminal motions, rapid variability, high observed brightness temperatures, detection of γ -ray emission).

The Synchrotron Self-Compton model (SSC, Ghisellini et al. 1993) poses a third observational constraint on the Doppler factor, by requiring that the X-ray flux produced by Inverse Compton does not exceed that observed. Thanks to the availability of a large number of observations carried out by X-ray satellites (*Einstein*, EXOSAT, *ROSAT*, ASCA, and *BeppoSAX*), Donato et al. (2001, see references therein) have collected fluxes at 1 keV for all the objects in the sample. The standard SSC formula (Marscher 1987) yields the Doppler factor as an inverse power of the VLBI core angular dimension; since VLBI cores are unresolved in our data, we find lower limits on δ . There are 20 sources where the result is not informative; however, for 11 sources we have mild limits on δ , as reported in Table 7. These limits provide useful constraints on the minimum velocity and the maximum angle allowed. Basically, these values are in good agreement with those required from the core enhancement argument; given the independence of the two estimates, this strengthens the conclusion that small to moderate angles to the line-of-sight and high velocity jets are characteristic of the objects in the sample.

We illustrate the resulting allowed angles in Fig. 8. The derived angles are consistent with the unified scheme, since most of the BL Lacs in our sample are oriented at a small to moderate angle to the line of sight. In Table 8, we present the resulting best available estimates from the previous studies of the allowed jet orientation angle θ and the relative Doppler factor δ in the case $\Gamma = 5$. We note that, despite the low number of LBLs considered here, they seem to be oriented at smaller angles ($\langle\theta\rangle_{\text{LBL}} = 14^\circ \pm 12^\circ$) with respect to HBLs ($\langle\theta\rangle_{\text{HBL}} = 25^\circ \pm 9^\circ$). A Kolmogorov-Smirnov test on the viewing angles for the two populations of HBL and LBL yields a probability $< 8 \times 10^{-3}$ that the data sets are drawn from the same distribution (K-S statistic $d = 1.66$). Notice however the rather large uncertainties, which are due to the small number of objects but also to a likely large scatter in the distribution of intrinsic angles.

The adoption of a single Lorentz factor can also be partly responsible for this result. Although the assumption of $\Gamma = 5$ is a good approximation of the real situation, we explore another approach, less restrictive than assuming a constant velocity for all the jets. In particular, we consider the relation $\Gamma \sim 1/\theta$, which corresponds to the maximum angle allowed for a given Doppler factor and is, in a statistical sense, the most likely situation.

We still make use of the P_c/P_t relation, in order to uniquely determine the values of β and θ . We show in Fig. 9 the histogram of the resulting angles and Lorentz factor distribution. The average angle for the sample is $\langle\theta\rangle = 18^\circ \pm 5^\circ$, without showing any relevant difference between LBL and HBL ($\langle\theta_{\text{LBL}}\rangle = 15^\circ \pm 7^\circ$ and $\langle\theta_{\text{HBL}}\rangle = 20^\circ \pm 4^\circ$, respectively). There are still four LBL that need to be oriented at rather small angles ($\theta < 15^\circ$), namely 0829+046 ($z = 0.180$), 1418+546 ($z = 0.152$), 2200+420 ($z = 0.070$), and 2254+074 ($z = 0.190$); however, their redshifts are typically larger than the average, so these may be more extreme and peculiar objects. In Fig. 9 (right panel), we also show the distribution of Lorentz factors: the majority of objects, including all HBLs, are distributed around $\Gamma = 3$. There are however four objects separated from the others, which have $\Gamma > 5$; these objects are the four LBLs mentioned above.

Depending on the assumptions made on the jet bulk velocity, we are left with two alternatives on the beaming properties of the jet: either our HBLs are viewed at somewhat larger angles than LBL, or the bulk velocity of the radio jets for the HBL population is intrinsically smaller. The former explanation has been put forward several times in the literature (e.g. Celotti et al. 1993; Jannuzzi, Smith, & Elston 1994), although it cannot satisfactorily account for *all* observed properties of BL Lacs (Sambruna, Maraschi, & Urry 1996; Rector & Stocke 2001). Conversely, the latter interpretation has been less explored and is puzzling, since constraints on smaller scales, and from other arguments (e.g. TeV γ -ray emission), require an opposite behaviour. However, we note that, on parsec scales, the study of proper motions have revealed superluminal components in EGRET sources (Jorstad et al. 2001) and subluminal or absent motion in TeV sources (Tingay & Edwards 2002; Piner & Edwards 2004). Thus, it is interesting to speculate that the emission of TeV photons taking place on even smaller scales may be responsible for energetic losses resulting in slower jets on radio scale. Another possible explanation for the decrease in jet velocity invokes the properties of the interstellar medium (ISM), which can vary among galaxies. Note that evidence of a strong jet deceleration within ~ 5 kpc from the core has been found in 3C 449 (Feretti et al. 1999), 3C 31 (Laing & Bridle 2002), M 87 (Biretta, Sparks, & Macchetto 1999), and 3C 264 (Baum et al. 1997; Lara et al. 2004).

Since samples of distant objects with large flux limits (e.g. the 1 Jy) have been studied in detail, it is worthwhile to compare some properties of the two populations. The value of the core dominance parameter $f = \frac{S_{\text{core}}}{S_{\text{ext}}}$ in our sample is $\langle f \rangle = 3.2$ (see Fig. 10). Actually, we excluded the three sources (1418+546, 1514–241, and 2254+074) in which the flux density of the core is larger than the total; this behaviour has to be ascribed to variability, and reminds us that this result needs to be considered with caution. However, this is true also for other samples and we do not expect it to affect the average properties of the sources in

our sample. The present low redshift BL Lac sample is less core-dominated than the EMSS and the 1 Jy; in the EMSS $\langle f \rangle \geq 4.2$ (Rector et al. 2000) and much larger values are observed in the bright 1 Jy BL Lacs (Rector & Stocke 2001). Correspondingly, the core is frequently associated with a resolved radio morphology, including halos, secondary components, and symmetric two-sided jets; this also suggests that kiloparsec scale jets may have different properties, being either non-relativistic or still mildly relativistic in different sources.

It is also interesting to discuss the difference in orientation with respect to more powerful objects by considering the amount of bending in the jets. In particular, large bending is suggestive of small angles, while straight jets are more common in the presence of a larger angle between the jet axis and the line-of-sight. In Fig. 7 we present the bending angle distribution in the 1 Jy sample⁵ and for the present sample, excluding those belonging to the 1 Jy sample. The histogram provides a comparison of the two populations, which indicates that high power BL Lacs show larger distortions than weak ones. The significance of the difference between the two distributions is quite strong (Kolmogorov-Smirnov of 1.42, with a probability that the two distribution are intrinsically similar $\lesssim 0.03$). It is tempting to speculate that this may be ascribed to a different jet orientation, with smaller viewing angles for more powerful and twisting sources. However, it is also possible to give a different interpretation for this occurrence of large bending, if we speculate that FR II have intrinsically more bent jets than FR I and that the 1 Jy sample has a parent population in which FR II radio galaxies are a significant fraction. Figure 11 shows the bending angle versus radio power for all the BL Lacs with available measurements of the bending (from the present work or the 1 Jy sample): there is a weak trend of larger bending in more powerful sources, with a correlation coefficient of $r = 0.42$. In particular, the lack of large bending in low power sources is remarkable.

Whilst FR II sources may contribute to the parent population of the 1 Jy sample (see also Rector & Stocke 2001), FR I radio galaxies are the best candidate to be the unbeamed counterpart of the objects in the present sample. From our estimate of the jet velocity and orientation, we can derive the intrinsic core radio power: $P_{c,i} = P_{c,o} \times \delta^{-(2+\alpha)}$. In Fig. 12 we present the distribution of the core and low frequency total radio power for the present sample and the sample of FR I and low power compact radio galaxies studied by Giovannini et al. (2001). The two samples cover the same range in low frequency total radio power (Fig. 12, left), as expected if FR Is are the parent population of BL Lacs. We note that the total radio power at 325 MHz should be an intrinsic source property since the core is self-absorbed

⁵The bending angles for the objects in the 1 Jy sample have been derived by us from maps on parsec and kpc scale published in several works, e.g. Cassaro et al. (1999, 2002); Rector & Stocke (2001); Fomalont et al. (2000); Shen et al. (1998)

and extended lobe emission dominates at low frequency. In the right panels, the shaded histograms represent the intrinsic core radio power distribution, while the overlaid dashed histograms refer to the observed power of the radio core. Despite a significant difference in the observed values, the distribution of the intrinsic core radio power is similar and in the same range, confirming that the intrinsic properties of the two populations are the same.

We conclude that in our sample the parent population is composed of FR I radio galaxies alone and that the fraction of FR IIs in the parent population of BL Lacs must be very small, if any. FR IIs that may be present in the 1 Jy sample must therefore be ascribed to the very large volume considered. In any case, their incidence may not be negligible among the most powerful LBL, which could have different properties.

6. CONCLUSIONS

In this paper we presented a new sample of nearby BL Lac objects with no selection bias on their nuclear radio properties. For sources without good data available in literature, we present new VLA and VLBA images. Many sources exhibit a resolved radio morphology as expected if BL Lacs are FR I radio galaxies oriented at small angles. A few objects show a WAT or HT morphology suggesting that they are radio galaxies belonging to cluster of galaxies. Most of the arcsecond core flux density is present in our VLBA images; this result implies that we have not missed considerable sub-arcsecond structure.

On the kiloparsec scale we have both symmetric and one-sided sources suggesting that kiloparsec scale jets may have different properties, being either non-relativistic or still mildly relativistic in different sources. This suggests that the decrease in jet velocity is related to the ISM properties which can vary among galaxies. More detailed studies with the EVLA or the proposed New Mexico Array are necessary to better investigate this possibility.

Confirming previous results by Rector et al. (2003), parsec and kiloparsec scale jets are oriented at the same PA in a large fraction of HBLs. Given the relative numbers of HBLs and LBLs in the sample, the low number of distorted structures and the core dominance argument, HBL sources show less distortion and therefore are expected to be oriented at larger angles than the LBL sources. This is confirmed by the core dominance argument, the jet/counterjet ratio, and the Synchrotron Self Compton model, under the assumption that all jets possess the same Lorentz factor $\Gamma = 5$. By contrast, if we allow both Γ and θ to vary, we derive similar orientation ($\langle\theta_{LBL}\rangle = 15^\circ \pm 7^\circ$ and $\langle\theta_{HBL}\rangle = 20^\circ \pm 4^\circ$) and a difference in velocity; interestingly, LBL would have larger bulk velocities (up to $\Gamma \lesssim 7$) than HBL, including TeV sources ($\langle\Gamma\rangle \sim 3$). In both cases, the Doppler factor of BL Lacs is

considerably smaller in the parsec scale radio jets than in the γ –ray emitting region.

In any case, we estimate that most sources ($\sim 80\%$) in our sample are oriented at an angle to the line-of-sight larger than 10° . The derived range in orientation correspond to a possible range of Doppler factors. From these values, we compute the relative intrinsic core radio power and show that intrinsic core radio powers are similar in BL Lacs and FR I radio galaxies and low power radio galaxies of the same range of total radio power. No FR II is allowed as the misaligned counterpart of a low redshift BL Lac.

We thank the referee Dr. Eric Perlman for many useful comments and suggestions which improved this work. We thank also D. Dallacasa and A. Treves for a critical reading of the paper and valuable suggestions. This research has made use of the NASA/IPAC Extragalactic Database (NED) which is operated by the Jet Propulsion Laboratory, Caltech, under contract with NASA and of NASA’s Astrophysics Data System (ADS) Bibliographic Services. MERLIN is a National Facility operated by the University of Manchester at Jodrell Bank Observatory on behalf of PPARC. This material is based upon work supported by the Italian Ministry for University and Research (MIUR) under grant COFIN 2003-02-7534.

REFERENCES

Aharonian, F., et al. 2002, A&A, 384, L23

Aharonian, F., et al. 2003, A&A, 406, L9

Anton, S., Browne I. W. A. , Marcha M. J. M., Bondi M., Polatidis A. 2004, MNRAS, in press (astro-ph/0404606)

Antonucci, R. R. J. & Ulvestad, J. S. 1985, ApJ, 294, 158

Appl, S., Sol, H., & Vicente, L. 1996, A&A, 310, 419

Attridge, J. M., Roberts, D. H., & Wardle, J. F. C. 1999, ApJ, 518, L87

Baum, S. A., et al. 1997, ApJ, 483, 178

Becker, R. H., White, R. L., & Helfand, D. J. 1995, ApJ, 450, 559

Biretta, J. A., Sparks, W. B., & Macchetto, F. 1999, ApJ, 520, 621

Caccianiga, A. & Marcha, M. J. M. 2004, MNRAS, 348, 937

Catanese, M. et al. 1998, *ApJ*, 501, 616

Cassaro, P., Stanghellini, C., Bondi, M., Dallacasa, D., della Ceca, R., & Zappalà, R. A. 1999, *A&AS*, 139, 601

Cassaro, P., Stanghellini, C., Dallacasa, D., Bondi, M., & Zappalà, R. A. 2002, *A&A*, 381, 378

Celotti, A., Maraschi, L., Ghisellini, G., Caccianiga, A., & Maccacaro, T. 1993, *ApJ*, 416, 118

Chiaberge, M., Celotti, A., Capetti, A., & Ghisellini, G. 2000, *A&A*, 358, 104

Condon, J. J., Cotton, W. D., Greisen, E. W., Yin, Q. F., Perley, R. A., Taylor, G. B., & Broderick, J. J. 1998, *AJ*, 115, 1693

Costamante, L. & Ghisellini, G. 2002, *A&A*, 384, 56

Danziger, I. J., Fosbury, R. A. E., Goss, W. M., & Ekers, R. D. 1979, *MNRAS*, 188, 415

Donato, D., Ghisellini, G., Tagliaferri, G., & Fossati, G. 2001, *A&A*, 375, 739

Donato, D., Gliozzi, M., Sambruna, R. M., & Pesce J. E. 2003, *A&A*, 407, 503

Douglas, J. N., Bash, F. N., Bozian, F. A., Torrence, G. W., & Wolfe, C. 1996, *AJ*, 111, 1945

Falomo, R., Kotilainen, J. K., & Treves, A. 2002, *ApJ*, 569, L35

Falomo, R. 1994, *The Messenger*, 77, 49

Falomo, R., Scarpa, R., & Bersanelli, M. 1994, *ApJS*, 93, 125

Falomo, R., Pesce, J. E., & Treves, A. 1995, *ApJ*, 438, L9

Falomo, R., Scarpa, R., Treves, A., & Urry, C. M. 2000, *ApJ*, 542, 731

Feretti, L., Perley, R., Giovannini, G., & Andernach, H. 1999, *A&A*, 341, 29

Fey, A. L. & Charlot, P. 2000, *ApJS*, 128, 17

Fomalont, E. B., Frey, S., Paragi, Z., Gurvits, L. I., Scott, W. K., Taylor, A. R., Edwards, P. G., & Hirabayashi, H. 2000, *ApJS*, 131, 95

Fossati, G., Maraschi, L., Celotti, A., Comastri, A., & Ghisellini, G. 1998, *MNRAS*, 299, 433

Gabuzda, D. C. & Cawthorne, T. V. 2003, MNRAS, 338, 312

Ghisellini, G., Padovani, P., Celotti, A., & Maraschi, L. 1993, ApJ, 407, 65

Ghisellini, G., Celotti, A., Fossati, G., Maraschi, L. & Comastri, A. 1998, MNRAS, 301, 451

Giovannini, G. 2003, NewAR, 47, 551

Giovannini, G., Feretti, L., Gregorini, L., & Parma, P. 1988, A&A, 199, 73

Giovannini, G., Feretti, L., Venturi, T., Lara, L., Marcaide, J., Rioja, M., Spangler, S. R., & Wehrle, A. E. 1994, ApJ, 435, 116

Giovannini, G., Cotton, W. D., Feretti, L., Lara, L., & Venturi, T. 2001, ApJ, 552, 508

Giovannini, G., Falomo, R., Scarpa, R., Treves, A., & Urry, C. M. 2004, ApJ, in press

Giroletti, M. et al. 2004, ApJ, 600, 127

Gómez, J. & Marscher, A. P. 2000, ApJ, 530, 245

Green, R. F., Schmidt, M., & Liebert, J. 1986, ApJS, 61, 305

Hanasz, M. & Sol, H. 1996, A&A, 315, 355

Holder, J. et al. 2003, ApJ, 583, L9

Homan, D. C., Ojha, R., Wardle, J. F. C., Roberts, D. H., Aller, M. F., Aller, H. D., & Hughes, P. A. 2001, ApJ, 549, 840

Horan, D. et al. 2002, ApJ, 571, 753

Jannuzzi, B. T., Smith, P. S., & Elston, R. 1994, ApJ, 428, 130

Jorstad, S. G., Marscher, A. P., Mattox, J. R., Wehrle, A. E., Bloom, S. D., & Yurchenko, A. V. 2001, ApJS, 134, 181

Keel, W. C. 1986, ApJ, 302, 296

Kollgaard, R. I., Gabuzda, D. C., & Feigelson, E. D. 1996, ApJ, 460, 174

Laing, R. A. & Bridle, A. H. 2002, MNRAS, 336, 1161

Landt, H., Padovani, P., Perlman, E. S., Giommi, P., Bignall, H., & Tzioumis, A. 2001, MNRAS, 323, 757

Lara, L., Giovannini, G., Cotton, W. D., Feretti, L., & Venturi, T. 2004, A&A, 415, 905

Laurent-Muehleisen, S. A., Kollgaard, R. I., Moellenbrock, G. A., & Feigelson, E. D. 1993, AJ, 106, 875

Lin, Y. C. et al. 1995, ApJ, 442, 96

Lister, M. L., Marscher, A. P., & Gear, W. K. 1998, ApJ, 504, 702

Marscher, A. P. 1987, Superluminal Radio Sources, 280

Meier, D. L. 2003, New Astronomy Review, 47, 667

Morganti, R., Killeen, N. E. B., & Tadhunter, C. N. 1993, MNRAS, 263, 1023

Morris, S. L., Stocke, J. T., Gioia, I. M., Schild, R. E., Wolter, A., Maccacaro, T., & della Ceca, R. 1991, ApJ, 380, 49

Murphy, D. W., Browne, I. W. A., & Perley, R. A. 1993, MNRAS, 264, 298

Nishiyama, T., et al. 2000, AIP Conf. Proc. 516, Proc. 26th International Cosmic Ray Conference, ed. B. L. Dingus, D. B. Kieda, & M. H. Salamon (Melville: AIP), 370

O'Dea, C. P., Barvainis, R., & Challis, P. M. 1988, AJ, 96, 435

Orr, M. J. L. & Browne, I. W. A. 1982, MNRAS, 200, 1067

Padovani, P. & Giommi, P. 1995, MNRAS, 277, 1477

Padovani, P., Perlman, E. S., Landt, H., Giommi, P., & Perri, M. 2003, ApJ, 588, 128

Perlman, E. S. 1994, Ph.D. Thesis, University of Colorado

Perlman, E. S. & Stocke, J. T. 1993, ApJ, 406, 430

Perlman, E. S. et al. 1996, ApJS, 104, 251

Perlman, E. S., Padovani, P., Giommi, P., Sambruna, R., Jones, L. R., Tzioumis, A., & Reynolds, J. 1998, AJ, 115, 1253

Perlman, E. S., Biretta, J. A., Zhou, F., Sparks, W. B., & Macchetto, F. D. 1999, AJ, 117, 2185

Perlman, E. S., Biretta, J. A., Sparks, W. B., Macchetto, F. D., & Leahy, J. P. 2001, ApJ, 551, 206

Pesce, J. E., Sambruna, R. M., Tavecchio, F., Maraschi, L., Cheung, C. C., Urry, C. M., & Scarpa, R. 2001, *ApJ*, 556, L79

Pian, E., Falomo, R., Ghisellini, G., Maraschi, L., Sambruna, R. M., Scarpa, R., & Treves, A. 1996, *ApJ*, 459, 169

Piccinotti, G., Mushotzky, R. F., Boldt, E. A., Holt, S. S., Marshall, F. E., Serlemitsos, P. J., & Shafer, R. A. 1982, *ApJ*, 253, 485

Piner, B. G. & Edwards, P. G. 2004, *ApJ*, in press (astro-ph/0309547)

Rector, T. A. & Stocke, J. T. 2001, *AJ*, 122, 565

Rector, T. A., Stocke, J. T., Perlman, E. S., Morris, S. L., & Gioia, I. M. 2000, *AJ*, 120, 1626

Rector, T. A., Gabuzda, D. C., & Stocke, J. T. 2003, *AJ*, 125, 1060

Reid, R. I., Kronberg, P. P., & Perley, R. A. 1999, *ApJS*, 124, 285

Remillard, R., et al. 1999, unpublished

Rengelink, R. B., Tang, Y., de Bruyn, A. G., Miley, G. K., Bremer, M. N., Roettgering, H. J. A., & Bremer, M. A. R. 1997, *A&AS*, 124, 259

Sambruna, R. M., Maraschi, L., & Urry, C. M. 1996, *ApJ*, 463, 444

Scarpa, R., Falomo, R., & Pian, E. 1995, *A&A*, 303, 730

Scarpa, R., Urry, C. M., Falomo, R., & Treves, A. 1999, *ApJ*, 526, 643

Scarpa, R., Urry, C. M., Falomo, R., Pesce, J. E., & Treves, A. 2000, *ApJ*, 532, 740

Schachter, J. F. et al. 1993, *ApJ*, 412, 541

Schwab, F. R. & Cotton, W. D. 1983, *AJ*, 88, 688

Shen, Z.-Q. et al. 1998, *AJ*, 115, 1357

Shepherd, M. C., Pearson, T. J., & Taylor, G. B. 1994, *BAAS*, 26, 987

Shepherd, M. C., Pearson, T. J., & Taylor, G. B. 1995, *BAAS*, 27, 903

Slinglend, K., Batuski, D., Miller, C., Haase, S., Michaud, K., & Hill, J. M. 1998, *ApJS*, 115, 1

Sol, H., Pelletier, G., & Asseo, E. 1989, MNRAS, 237, 411

Sparks, W. B., Biretta, J. A., & Macchetto, F. 1994, ApJS, 90, 909

Stickel, M., Fried, J. W., Kuehr, H., Padovani, P., & Urry, C. M. 1991, ApJ, 374, 431

Stickel, M. & Kuehr, H. 1994, A&AS, 103, 349

Stocke, J. T., Morris, S. L., Gioia, I. M., Maccacaro, T., Schild, R., Wolter, A., Fleming, T. A., & Henry, J. P. 1991, ApJS, 76, 813

Tavecchio, F., Maraschi, L., & Ghisellini, G. 1998, ApJ, 509, 608

Tingay, S. J. & Edwards, P. G. 2002, AJ, 124, 652

Urry, C. M. & Padovani, P. 1995, PASP, 107, 803

Urry, C. M., Scarpa, R., O'Dowd, M., Falomo, R., Pesce, J. E., & Treves, A. 2000, ApJ, 532, 816

Veron-Cetty, M.-P. & Veron, P. 1993, A&AS, 100, 521

Wardle, J. F. C., Moore, R. L., & Angel, J. R. P. 1984, ApJ, 279, 93

Wrobel, J. M. & Lind, K. R. 1990, ApJ, 348, 135

Table 1. Objects in the Sample

Num.	Name (IAU)	Other Name	z	RA	Dec	Class	Sample
1	0145+138		0.125	01 48 29.7	+14 02 18	H	Slew
2	0229+200		0.140	02 32 48.4	+20 17 16	H	HEAO-A3
3	0347–121		0.188	03 49 23.2	–11 59 27	H	HEAO-A3
4	0350–371		0.165	03 51 53.8	–37 03 46	H	EMSS
5	0521–365		0.055	05 22 58.0	–36 27 31	L	HEAO-A3
6	0548–322		0.069	05 50 40.8	–32 16 18	H	HEAO-A2
7	0706+591		0.125	07 10 30.0	+59 08 20	H	HEAO-A3
8	0806+524		0.137	08 09 49.1	+52 18 59	H	Slew
9	0829+046		0.180	08 31 48.9	+04 29 39	L	HEAO-A3
10	0927+500		0.188	09 30 37.6	+49 50 26	H	Slew
11	1101+384	Mkn 421	0.031	11 04 27.3	+38 12 32	H	HEAO-A3
12	1133+704	Mkn 180	0.046	11 36 26.4	+70 09 27	H	HEAO-A3
13	1212+078		0.136	12 15 10.9	+07 32 04	H	Slew
14	1215+303		0.130	12 17 52.1	+30 07 01	H	Slew
15	1218+304		0.182	12 21 21.9	+30 10 37	H	HEAO-A2
16	1229+643		0.164	12 31 31.4	+64 14 18	H	EMSS
17	1255+244		0.141	12 57 31.9	+24 12 40	H	Slew
18	1418+546	OQ 530	0.152	14 19 46.6	+54 23 15	L	PG
19	1426+428		0.129	14 28 32.6	+42 40 21	H	HEAO-A3
20	1440+122		0.162	14 42 48.2	+12 00 40	H	Slew
21	1514–241	AP Lib	0.049	15 17 41.8	–24 22 19	H	1 Jy
22	1652+398	Mkn 501	0.034	16 53 52.2	+39 45 37	H	1 Jy
23	1728+502	I Zw 187	0.055	17 28 18.6	+50 13 10	H	HEAO-A3
24	1807+698	3C 371	0.051	18 06 50.6	+69 49 28	L	1 Jy
25	1959+650		0.048	19 59 59.8	+65 08 55	H	HEAO-A3
26	2200+420	BL Lac	0.070	22 02 43.3	+42 16 40	L	1 Jy
27	2201+044		0.027	22 04 17.6	+04 40 02	L	HEAO-A3
28	2254+074		0.190	22 57 17.3	+07 43 12	L	1 Jy
29	2344+514		0.044	23 47 04.8	+51 42 18	H	Slew
30	2356–309		0.165	23 59 07.8	–30 37 40	H	HEAO-A3

Note. — Col. 7: H – High frequency peaked BL Lac, L – Low frequency peaked BL Lac. Col. 8: 1 Jy (Stickel et al. 1991); HEAO-A2 (Piccinotti et al. 1982); HEAO-A3 (Remillard et al. 1999); EMSS (Morris et al. 1991); Slew (Schachter et al. 1993; Perlman et al. 1996)

Table 2. Summary of 1.4 GHz VLA Observations

Date	Conf.	hrs.	Targets
2002 Feb 22	A	5	0706+591, 0806+524, 0829+046, 0927+500, 1133+704, 1212+078, 1218+304, 1229+643, 1255+244, 1426+428, 1728+502, 1959+650
2002 May 03	A	2.5	0145+138, 0229+200, 0347–121, 0350–371, 2254+074, 2344+514, 2356–309
2002 Oct 08	C	4.5	0145+138, 0229+200, 0347–121, 1728+502, 1807+698, 1959+650, 2254+074, 2344+514, 2356–309

Table 3. Summary of 5 GHz VLBA Observations

Date	hrs	Targets
2002 Feb 17	6	0145+138, 0229+200, 0347–121, 0350–371, 2344+514, 2356–309
2002 Feb 18	4	0521–365, 0548–322, 0706+591, 0806+524
2002 Feb 19	5	1212+078, 1218+304, 1229+643, 1255+244, 1440+122

Table 4. Image Parameters

Num.	Name	VLA (A conf.)		VLA (C conf.)		VLBA	
		noise	peak	noise	peak	noise	peak
1	0145+138	0.15	2.8	0.24	11.2	0.55	3.5
2	0229+200	0.30	40.4	0.35	52.9	0.49	15.7
3	0347-121	0.30	8.7	0.50	10.4	0.53	7.7
4	0350-371	0.30	22.3	0.72	11.9
5	0521-365	5.50	1034.9
6	0548-322	0.90	33.3
7	0706+591	0.15	62.6	0.38	33.2
8	0806+524	0.20	157.6	0.38	78.9
9	0829+046	0.25	736.2
10	0927+500	0.11	19.9
12	1133+704	0.18	111.6
13	1212+078	0.12	83.2	0.36	33.1
15	1218+304	0.20	65.6	0.41	44.1
16	1229+643	0.12	53.0	0.61	19.6
17	1255+244	0.10	6.5	0.55	2.9
19	1426+428	0.10	31.9
20	1440+122	0.47	17.1
23	1728+502	0.30	201.0	0.30	196.7
24	1807+698	0.60	1348.8
25	1959+650	0.25	198.5	0.24	241.2
28	2254+074	0.30	407.0	0.90	490.4
29	2344+514	0.30	195.8	0.40	220.2	0.39	89.7
30	2356-309	0.25	39.2	0.30	40.2	0.66	14.2

Note. — Noise levels and peak flux densities for Fig. 2 and 3 (Col. 3, 4), for Fig. 4 (Col. 5, 6), and for Fig. 6 (Col. 7, 8). All units are mJy/beam.

Table 5. Flux Densities

Num.	Name (IAU)	z	$S_{325\text{MHz}}$ (mJy)	$S_{\text{t},1.4\text{GHz}}$ (mJy)	$S_{\text{c},1.4\text{GHz}}$ (mJy)	c/tot	$S_{\text{c},5\text{GHz}}$ (mJy)	ref.	morph.
1	0145+138	0.125	$42 \pm 8^{\text{a}}$	35.8	3	0.08	2.1	(1)	j
2	0229+200	0.140	$110 \pm 22^{\text{a}}$	94.2	42	0.44	45	(1)	x
3	0347–121	0.188	$30 \pm 6^{\text{a}}$	25.7	9	0.35	8.4	(1)	j
4	0350–371	0.165	$46 \pm 9^{\text{a}}$	40.1	23	0.57	17	(2)	c
5	0521–365	0.055	$42920 \pm 480^{\text{b}}$	17620	3124 ^d	0.18	2581	(3)	x
6	0548–322	0.069	$1463 \pm 293^{\text{c}}$	505	76 ^e	0.15	68	(4)	w
7	0706+591	0.125	371 ± 3.8	160	65	0.41	80	(5)	j
8	0806+524	0.137	165 ± 4.1	183	160	0.87	172	(1)	c
9	0829+046	0.180	$671 \pm 31^{\text{c}}$	1257	643 ^d	0.51	1230	(6)	w
10	0927+500	0.188	12 ± 3.7	22.3	21	0.94	18	(1)	c
11	1101+384	0.031	1374 ± 3.3	889	548 ^e	0.62	640	(7)	j
12	1133+704	0.046	529 ± 5.2	337	115	0.34	125	(8)	h
13	1212+078	0.136	$175 \pm 35^{\text{a}}$	150	85	0.57	91	(1)	c
14	1215+303	0.130	1175 ± 2.9	593	355 ^d	0.60	445	(9)	h
15	1218+304	0.182	82 ± 2.7	71.3	67	0.94	56	(9)	c
16	1229+643	0.164	72 ± 3.7	63	55	0.87	42	(10)	c
17	1255+244	0.141	$19 \pm 4^{\text{a}}$	16.6	6.5	0.39	6.9	(1)	c
18	1418+546	0.152	962 ± 3.4	835	1058 ^d	1.27	1189	(11)	x
19	1426+428	0.129	64 ± 3.1	61.3	32	0.52	22	(8)	h
20	1440+122	0.162	$80 \pm 16^{\text{a}}$	68.5	60	0.87	41	(1)	c
21	1514–241	0.049	$1792 \pm 43^{\text{c}}$	2177	2562 ^d	1.18	1480	(12)	x
22	1652+398	0.034	1936 ± 4.7	1630	1376 ^d	0.84	1250	(7)	j
23	1728+502	0.055	317 ± 4.2	232	200	0.86	134	(8)	j
24	1807+698	0.051	4015 ± 4.4	2129	1350 ^d	0.63	1507	(13)	h
25	1959+650	0.048	252 ± 3.5	260	200	0.77	252	(1)	j
26	2200+420	0.070	1819 ± 4.1	6250	3310 ^d	0.53	4857	(9)	x
27	2201+044	0.027	$1222 \pm 58^{\text{c}}$	835	179 ^d	0.21	168	(8)	j
28	2254+074	0.190	$405 \pm 25^{\text{c}}$	404	405	1.00	1216	(9)	c
29	2344+514	0.044	569 ± 4.2	410	196	0.48	212	(1)	x

Table 5—Continued

Num.	Name (IAU)	z	$S_{325\text{MHz}}$ (mJy)	$S_{t,1.4\text{GHz}}$ (mJy)	$S_{c,1.4\text{GHz}}$ (mJy)	c/tot	$S_{c,5\text{GHz}}$ (mJy)	ref.	morph.
30	2356–309	0.165	75 ± 15^a	66.2	39	0.59	29 (5)		x

Note. — Col. 4: total source flux density at 325 MHz from the WENSS, except as noted: (a) extrapolated from the 1.4 GHz flux density (Col. 5) with $\alpha = 0.11$, (b) interpolated from NED data between 80 and 8800 MHz, (c) Texas Survey (Douglas et al. 1996). Col 5: total source flux density at 1.4 GHz from the NVSS. Col 6: arcsecond core flux density at 1.4 GHz from VLA A configuration data or (d) Antonucci & Ulvestad (1985), (e) Laurent-Muehleisen et al. (1993). Col. 7: ratio between core and total flux density at 1.4 GHz. Col 8: arcsecond core flux density at 5 GHz, with references as given in Col. 9. Col. 9: (1) Perlman et al. (1996), (2) Veron-Cetty & Veron (1993), (3) interpolated from data between 1.4 GHz and 15 GHz, (4) Reid et al. (1999), (5) NED, (6) MERLIN archive data, (7) Giovannini et al. (2001), (8) Laurent-Muehleisen et al. (1993), (9) Fossati et al. (1998), (10) Padovani & Giommi (1995), (11) Murphy et al. (1993), (12) Morganti et al. (1993), (13) Cassaro et al. (1999). Col. 10: (c) unresolved; (j) core+jet(s), (h) core+halo, (x) extended, complex structure, (w) wide angle tail

Table 6. VLBA data @5 GHz

Num.	Name	z	S_t (mJy)	S_c (mJy)	$S_{t,\text{mas}}/S_{c,''}$	B_j (mJy/beam)	PA_{jet} ($^{\circ}$)	R (\geq)	$\beta \cos \theta$ (\geq)	ref.
1	0145+138	0.125	3.3	3.2	1.61	(1)
2	0229+200	0.140	18.2	17.0	0.40	(1)
3	0347-121	0.188	8.5	8.1	1.01	(1)
4	0350-371	0.165	16.9	14.0	0.99	2.40	46	8	...	(1)
5	0521-365	0.055	1747	995.0	0.68	142.5	-44	119	0.74	(1)
6	0548-322	0.069	41.7	36.3	0.61	(1)
7	0706+591	0.125	42.0	33.8	0.53	3	-158	25	...	(1)
8	0806+524	0.137	136.8	66.0	0.80	40	20	333	0.82	(1)
9	0829+046	0.180	740	440.0	0.60	90	65	90	...	(2)
10	0927+500	0.188
11	1101+384	0.031	400	200	0.63	10	-32	100	0.73	(3)
12	1133+704	0.046	137.9	82.7	1.10	9.5	105	16	...	(4)
13	1212+078	0.136	50.0	34.5	0.53	3.0	92	23	...	(1)
14	1215+303	0.130	372.0	276.0	0.84	9.4	140	157	0.77	(3)
15	1218+304	0.182	56.9	39.8	1.02	3.2	73	25	...	(1)
16	1229+643	0.164	35.7	26.9	0.85	5.0	-43	28	...	(1)
17	1255+244	0.141	2.8	2.8	0.40	(1)
18	1418+546	0.152	1090	209.0	0.92	40	120	40	...	(5)
19	1426+428	0.129	21.2	19.1	0.96	2.1	20	3	...	(4)
20	1440+122	0.162	18.5	17.2	0.45	(1)
21	1514-241	0.049	2278	1948	1.49	253	161	90	...	(6)
22	1652+398	0.034	1118	491	0.89	100	150	400	0.83	(7)
23	1728+502	0.055	171	110.0	1.28	18.0	-55	200	0.79	(3)
24	1807+698	0.051	780	560.0	0.52	50	-102	38	...	(2)
25	1959+650	0.048	220	181.7	0.87	1.6	-5	8	...	(8)
26	2200+420	0.070	2164	1148	0.45	300	-170	350	0.82	(9)
27	2201+044	0.027	170	131.3	1.01	3.0	-42	3	...	(4)
28	2254+074	0.190	350	280.0	0.29	38.4	-120	43	...	(2)
29	2344+514	0.044	116.7	70.0	0.55	3.0	142	25	...	(1)
30	2356-309	0.165	21.9	21.9	0.76	(1)

Note. — Col. 4: Correlated VLBI flux density at 5 GHz. Col. 5: VLBI core flux density. Col. 6: Ratio between total VLBI flux density and arcsecond core at 5 GHz (Col. 8 in 4. Col. 7: Jet brightness near the core. Col. 8: Jet P.A. Col. 9: Lower limit for the jet/counterjet ratio. Col. 10: Estimated lower limit for $\beta \cos \theta$. Col. 11: References – (1) present work, (2) Fey & Charlot (2000), (3) Giroletti et al., in prep., (4)

Kollgaard et al. (1996), (5) Cassaro et al. (2002), (6) Fomalont et al. (2000), (7) Giroletti et al. (2004), (8) Rector et al. (2003), (9) Gabuzda & Cawthorne (2003)

Table 7. Limits from the Synchrotron Self Compton model

Name	δ_{\min}	Γ_{\min}	θ_{\max} ($^{\circ}$)
0521-365	2.2	1.3	27
0829+046	4.6	2.4	13
1101+384	2.4	1.4	25
1215+303	2.6	1.5	22
1418+546	2.2	1.3	26
1514-241	9.3	4.7	6
1652+398	2.5	1.4	24
1807+698	5.3	2.7	11
2200+420	6.7	3.4	9
2201+044	1.1	1.1	65
2254+074	4.0	2.1	15

Note. — Col. 2: Minimum Doppler factor from SSC (we only report sources where $\delta_{\min} > 1$). Col. 3: Minimum Lorentz factor Γ . Col. 4: Largest possible orientation angle.

Table 8. Final intrinsic parameters with $\Gamma = 5$

Num.	Name	$\log P_t$ W Hz $^{-1}$	$\Delta\theta_5$ ($^{\circ}$)	$\Delta\delta_5$	$\Delta P_{c,i}$ W Hz $^{-1}$
1	0145+138	24.17	41 – 61	0.4 – 0.8	23.10 – 23.70
2	0229+200	24.69	19 – 29	1.4 – 2.8	23.42 – 24.02
3	0347–121	24.39	23 – 35	1.0 – 2.0	23.24 – 23.84
4	0350–371	24.46	21 – 32	1.2 – 2.4	23.28 – 23.88
5	0521–365	26.45	21 – 27	1.5 – 2.3	24.51 – 24.86
6	0548–322	25.19	32 – 48	0.6 – 1.2	23.73 – 24.33
7	0706+591	25.12	21 – 32	1.2 – 2.4	23.69 – 24.29
8	0806+524	24.85	12 – 21	2.4 – 4.7	23.52 – 24.12
9	0829+046	25.70	3 – 13	4.6 – 9.1	24.05 – 24.65
10	0927+500	23.99	15 – 24	2.0 – 3.9	22.99 – 23.59
11	1101+384	24.46	19 – 25	1.8 – 2.7	23.28 – 23.63
12	1133+704	24.39	25 – 37	0.9 – 1.8	23.23 – 23.83
13	1212+078	24.87	16 – 26	1.7 – 3.4	23.53 – 24.13
14	1215+303	25.65	14 – 22	2.1 – 4.0	24.02 – 24.57
15	1218+304	24.80	15 – 24	1.9 – 3.7	23.49 – 24.09
16	1229+643	24.65	17 – 27	1.6 – 3.2	23.40 – 24.00
17	1255+244	23.93	24 – 37	0.9 – 1.9	22.95 – 23.55
18	1418+546	25.71	7 – 15	3.7 – 7.5	24.05 – 24.65
19	1426+428	24.38	22 – 33	1.1 – 2.2	23.23 – 23.83
20	1440+122	24.68	17 – 27	1.5 – 3.1	23.42 – 24.02
21	1514–241	24.97	0 – 6	7.7 – 9.9	22.90 – 23.11
22	1652+398	24.69	16 – 24	1.9 – 3.5	23.42 – 23.93
23	1728+502	24.32	21 – 32	1.2 – 2.4	23.19 – 23.79
24	1807+698	25.36	0 – 11	5.3 – 9.9	22.94 – 23.48
25	1959+650	24.10	16 – 26	1.7 – 3.3	23.06 – 23.66
26	2200+420	25.29	3 – 9	6.4 – 9.2	23.80 – 24.11
27	2201+044	24.28	30 – 44	0.7 – 1.3	23.17 – 23.77
28	2254+074	25.53	0 – 11	5.4 – 9.9	24.02 – 24.54
29	2344+514	24.38	21 – 32	1.2 – 2.3	23.23 – 23.83
30	2356–309	24.67	19 – 30	1.3 – 2.7	23.41 – 24.01

Table 8—Continued

Num.	Name	$\log P_t$ W Hz $^{-1}$	$\Delta\theta_5$ ($^{\circ}$)	$\Delta\delta_5$	$\Delta P_{c,i}$ W Hz $^{-1}$

Note. — Col. 3: Logarithm of total radio power at 325 MHz. Col. 4: range of possible jet orientation angle. Col. 5: Doppler factor range. Col. 6: Logarithm of intrinsic core radio power at 5 GHz.

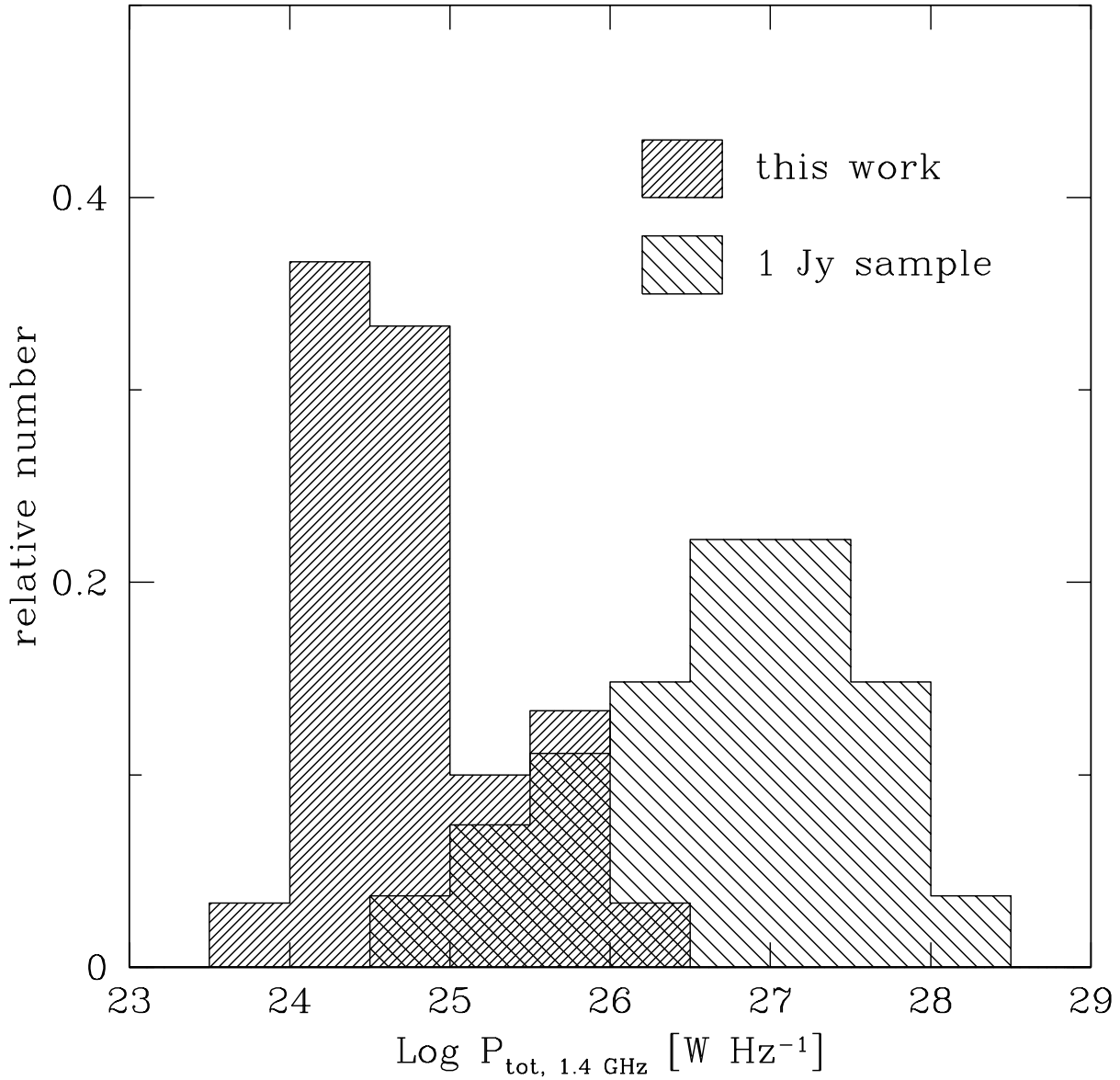


Fig. 1.— Histogram of total power distribution at 1.4 GHz for objects in our sample and in the 1 Jy sample. Data from the NVSS survey (Condon et al. 1998) for our sample and from Rector & Stocke (2001) for the 1 Jy sample.

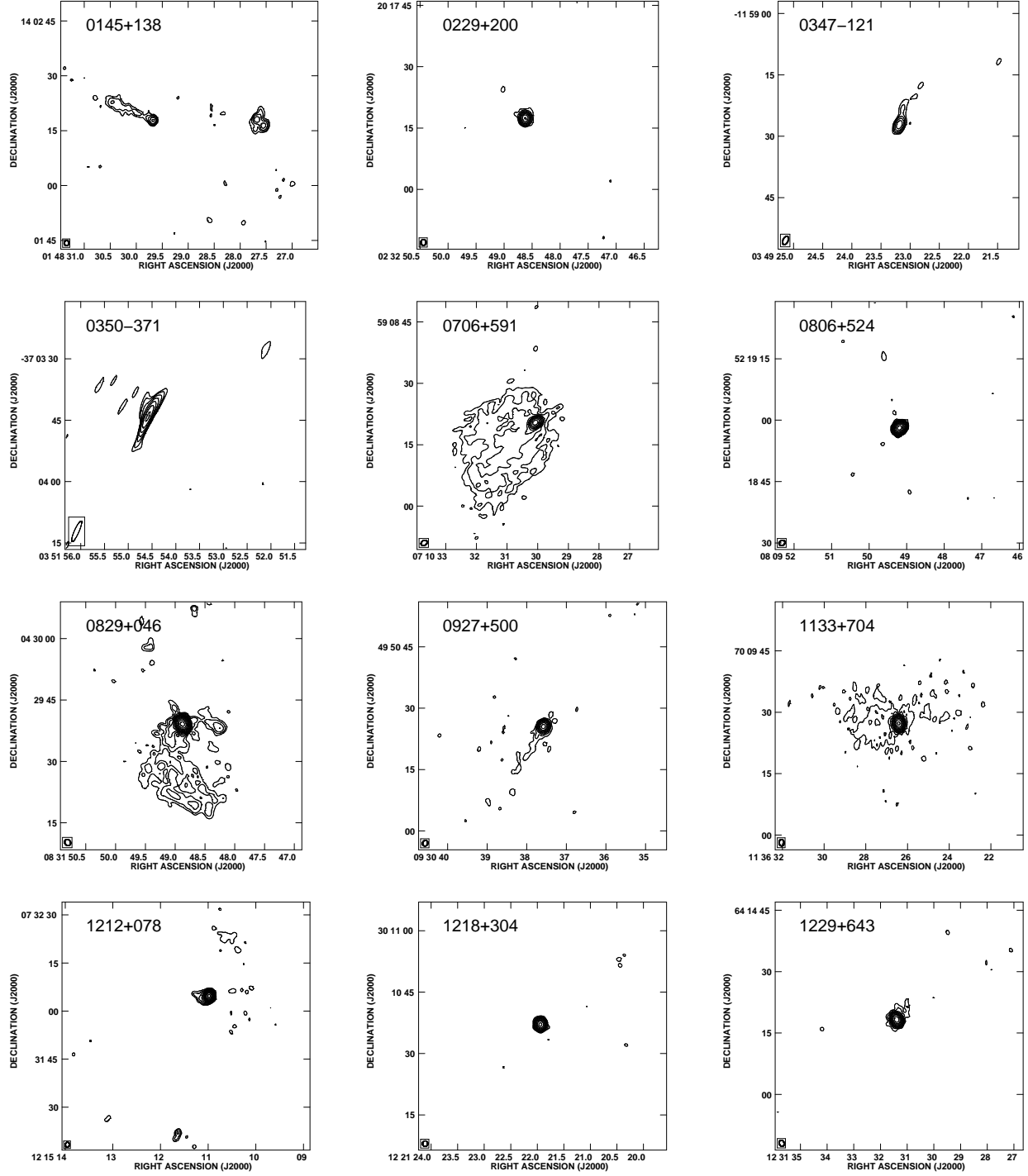


Fig. 2.— VLA images taken in A configuration page 1 of 2. Contours are drawn at (1, 2, 4, 8, 16, ...) times the noise level. Noise levels and image peaks are given in Tab. 4.

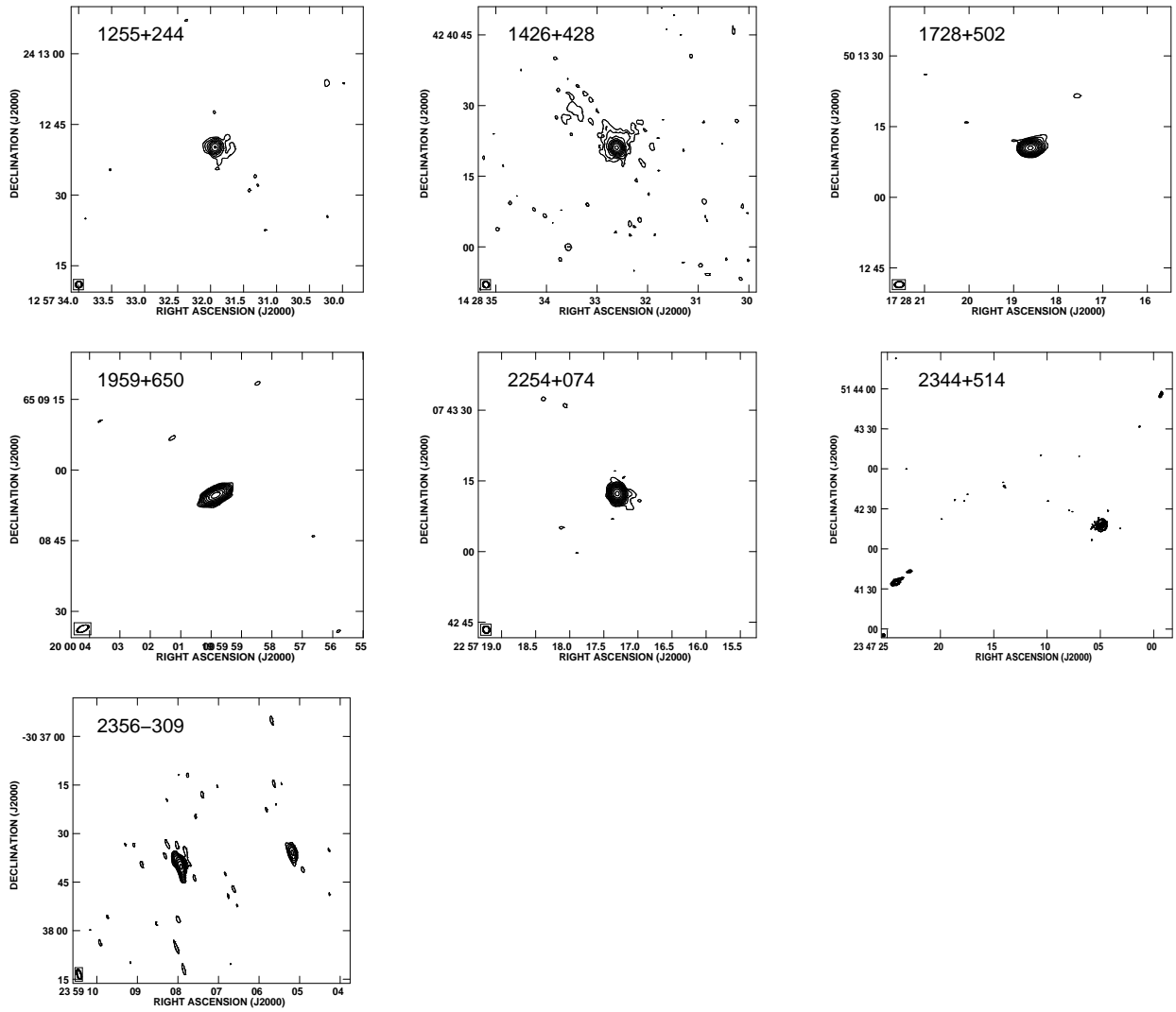


Fig. 3.— VLA images taken in A configuration continued. Contours are drawn at (1, 2, 4, 8, 16, ...) times the noise level. Noise levels and image peaks are given in Tab. 4.

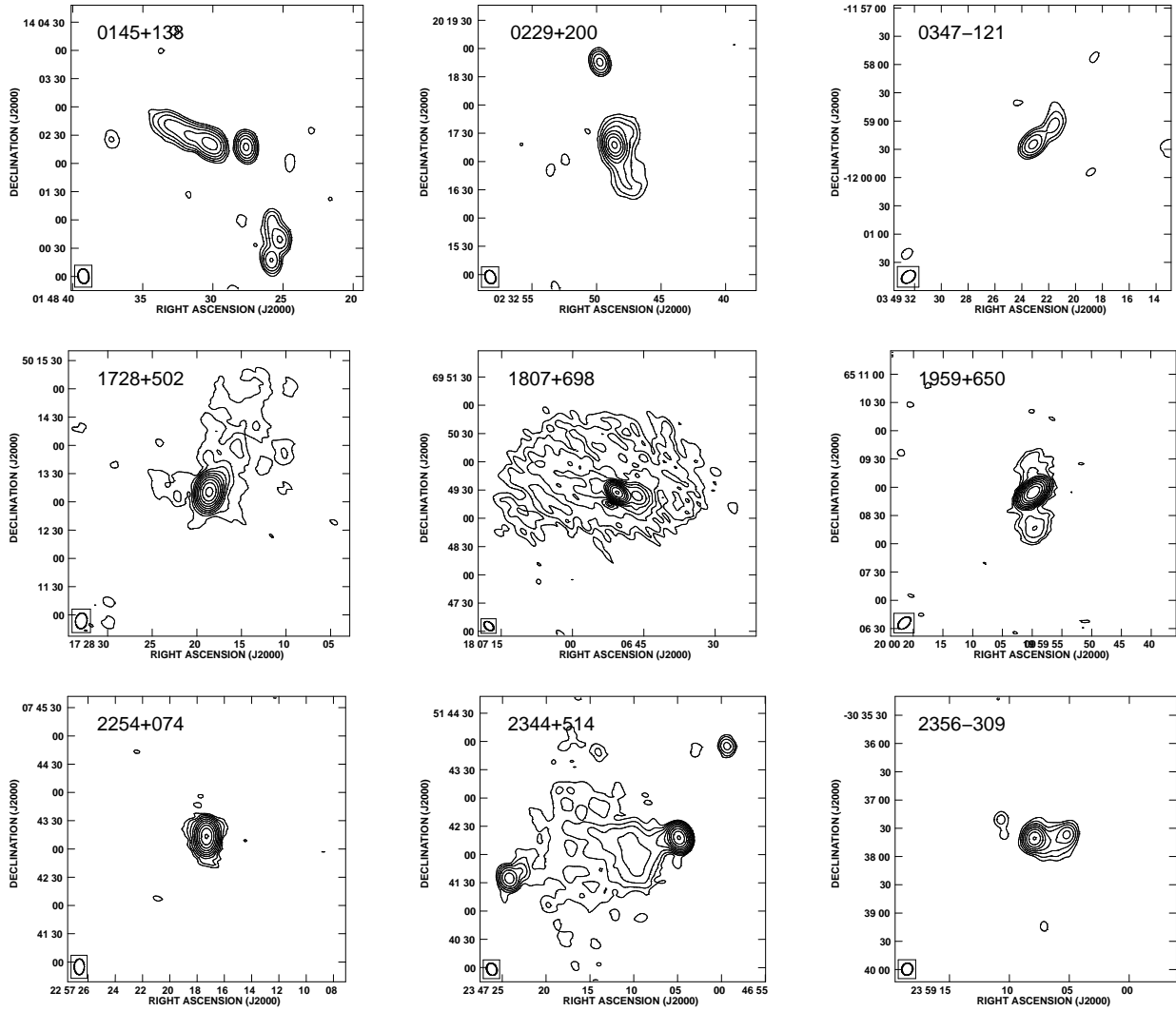


Fig. 4.— VLA images taken in C configuration. Contours are drawn at (1, 2, 4, 8, 16, ...) times the noise level. Noise levels and image peaks are given in Tab. 4.

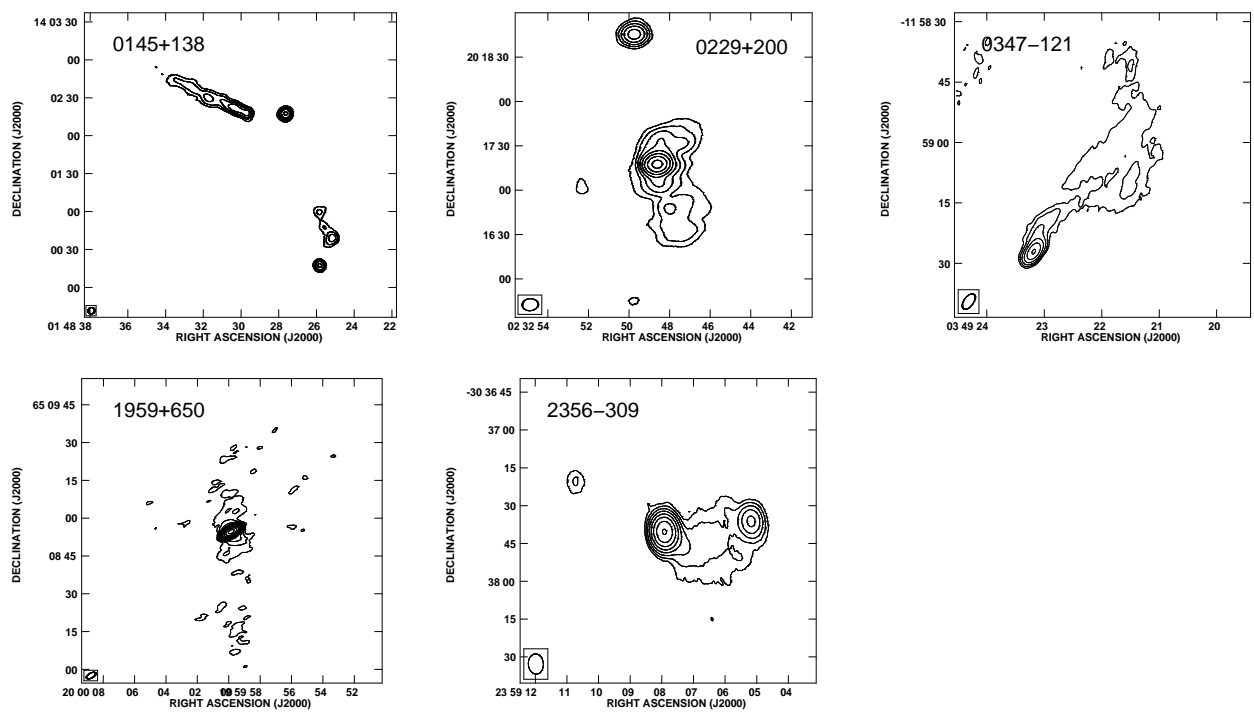


Fig. 5.— VLA images made from a combination of data from the A and C configurations.

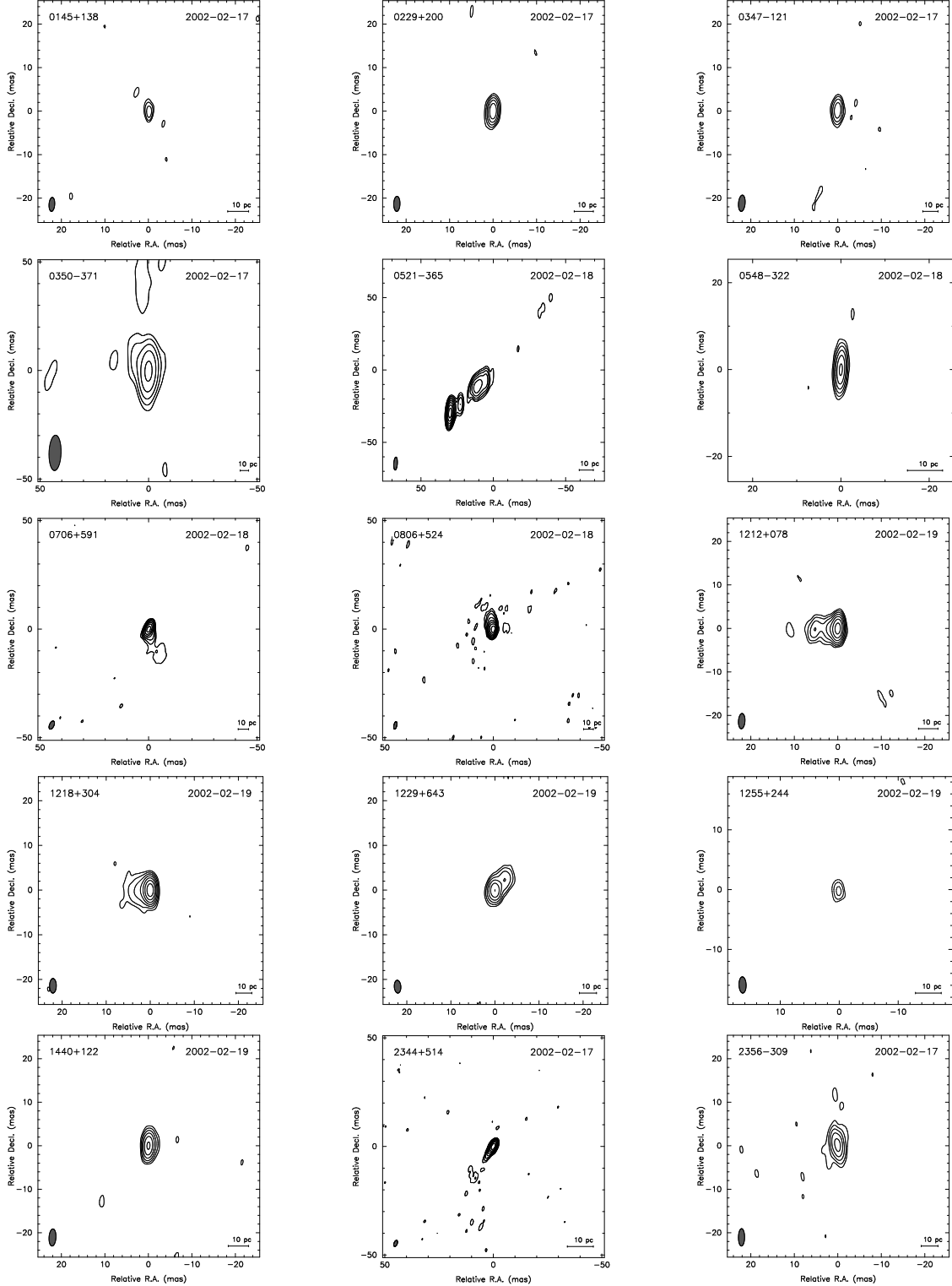


Fig. 6.— VLBA images. Contours are drawn at (1, 2, 4, 8, 16, ...) times the noise level. Noise level and image peaks are given in Tab. 4.

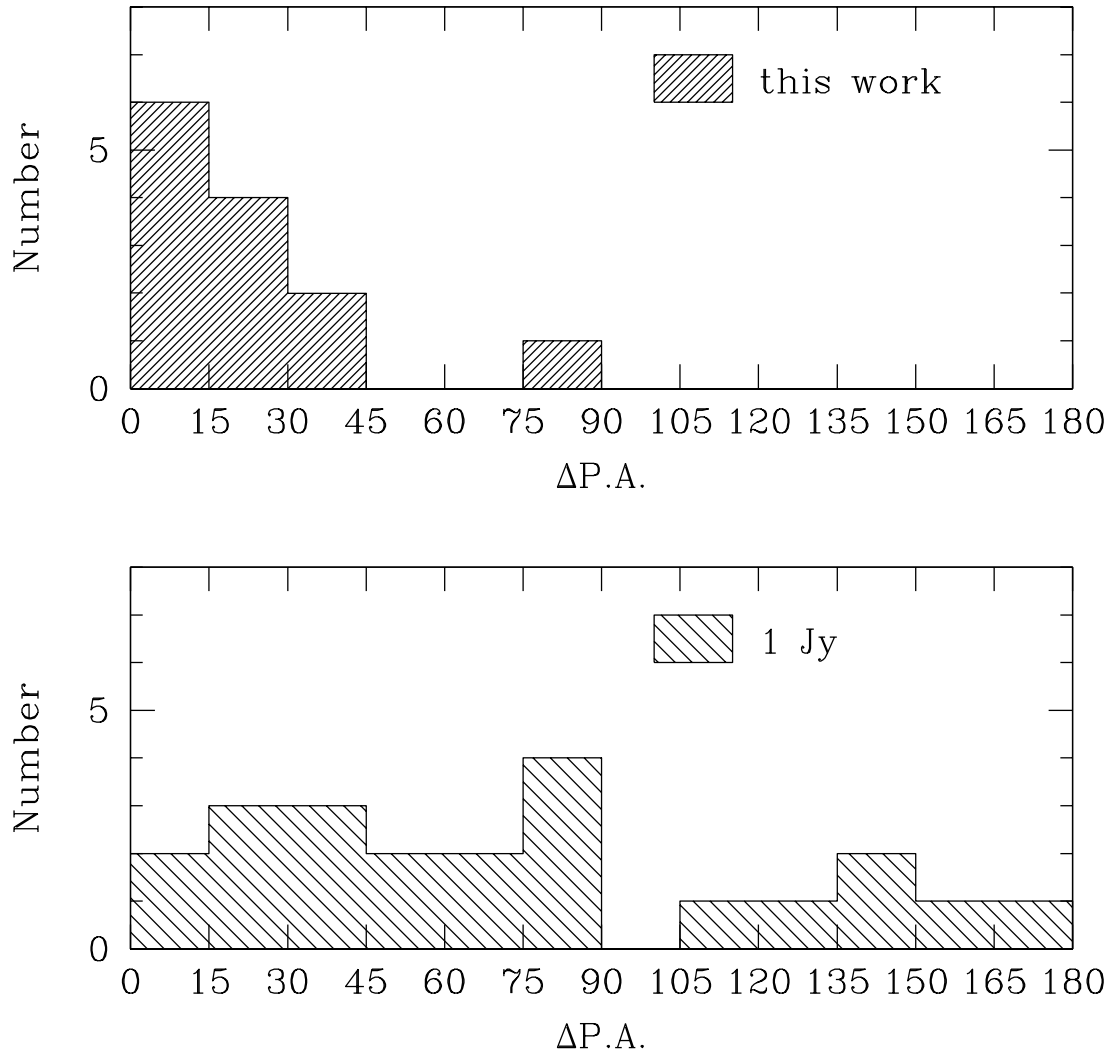


Fig. 7.— Distribution of bending for sources in the present sample (top) and in the 1 Jy sample (bottom, see text). We have excluded from our sample objects belonging to the 1 Jy sample.

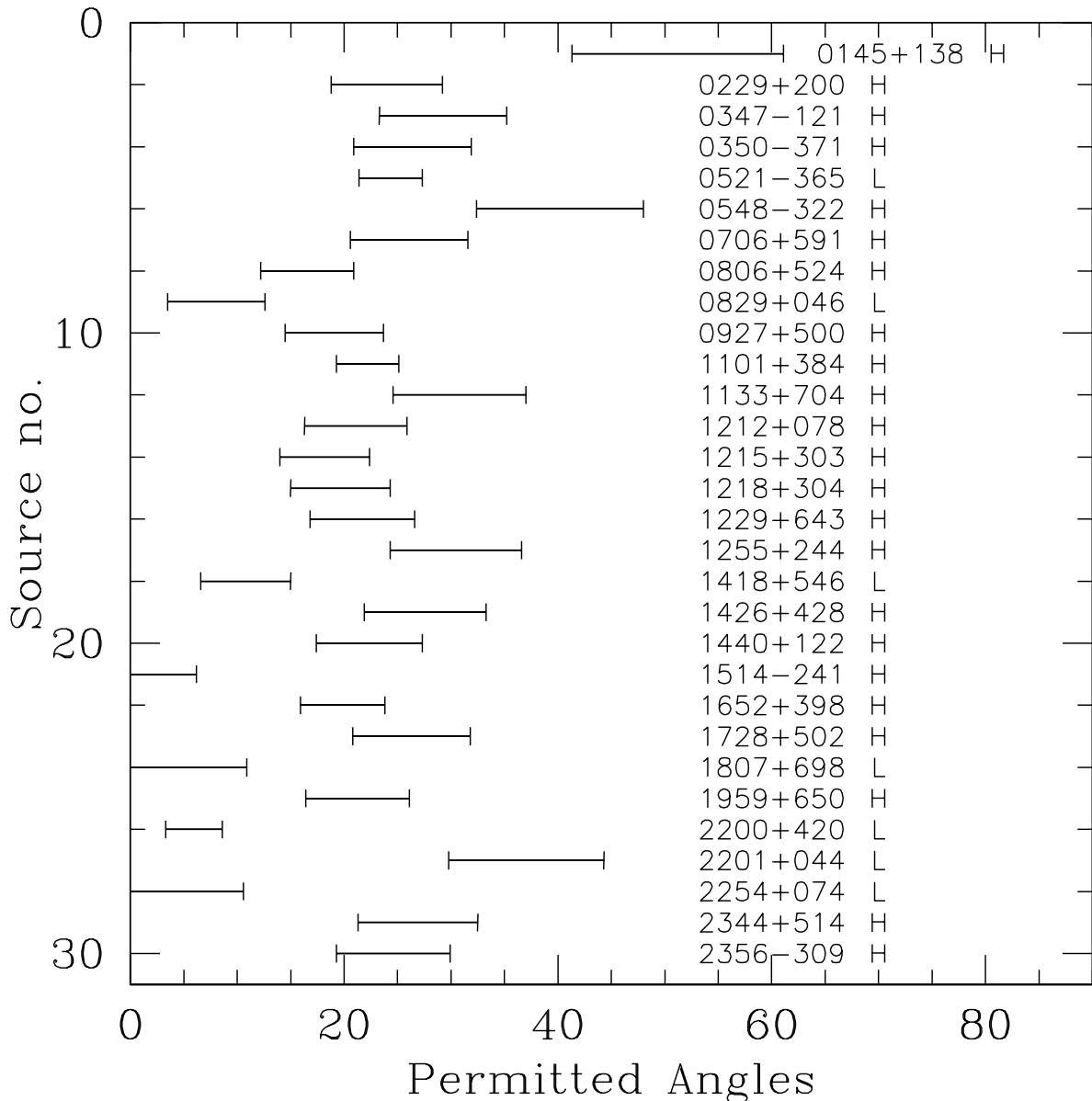


Fig. 8.— Allowed angles to the line-of-sight, assuming $\Gamma = 5$. The letter beside the name refers to the type of source (H: high frequency peaked BL Lac; L: low frequency peaked BL Lac).

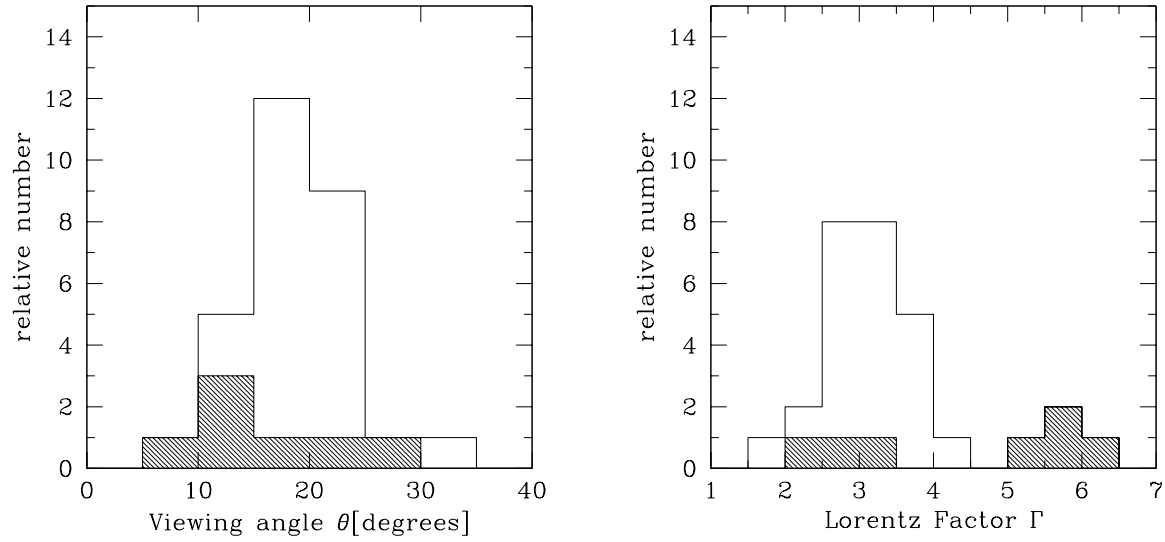


Fig. 9.— Distribution of the resulting viewing angle θ (left) and Lorentz factor Γ (right), assuming $\Gamma \sim 1/\theta$; the shaded parts correspond to LBL only.

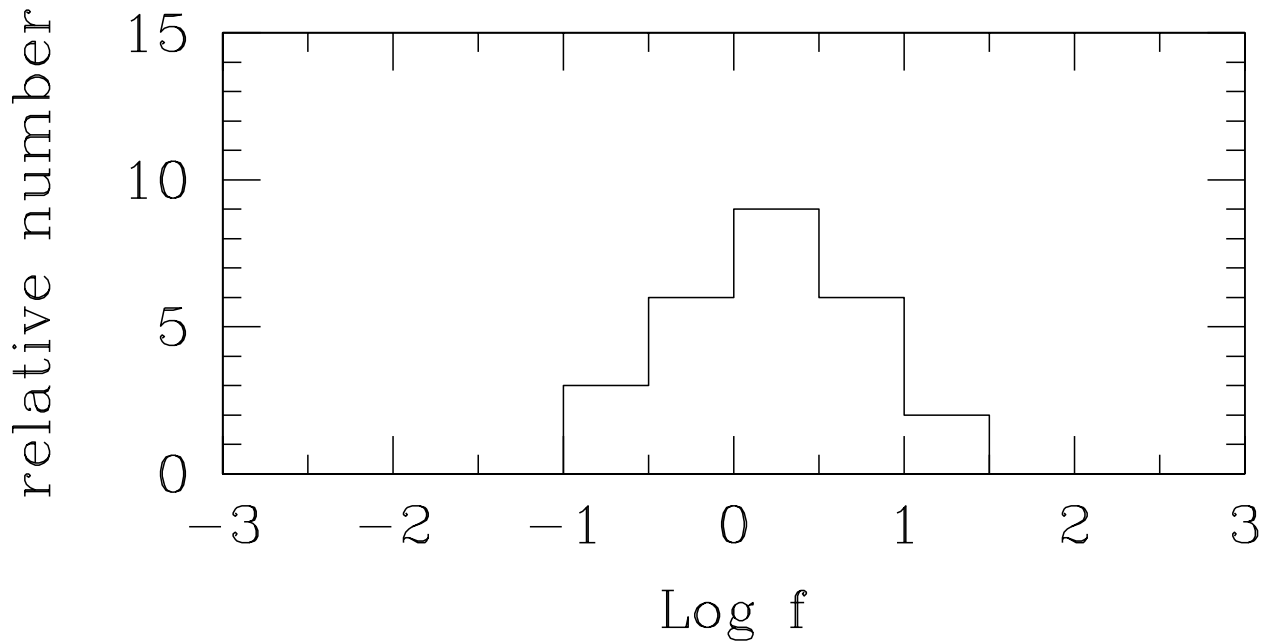


Fig. 10.— Distribution of the core dominance factor f for sources in the present sample.

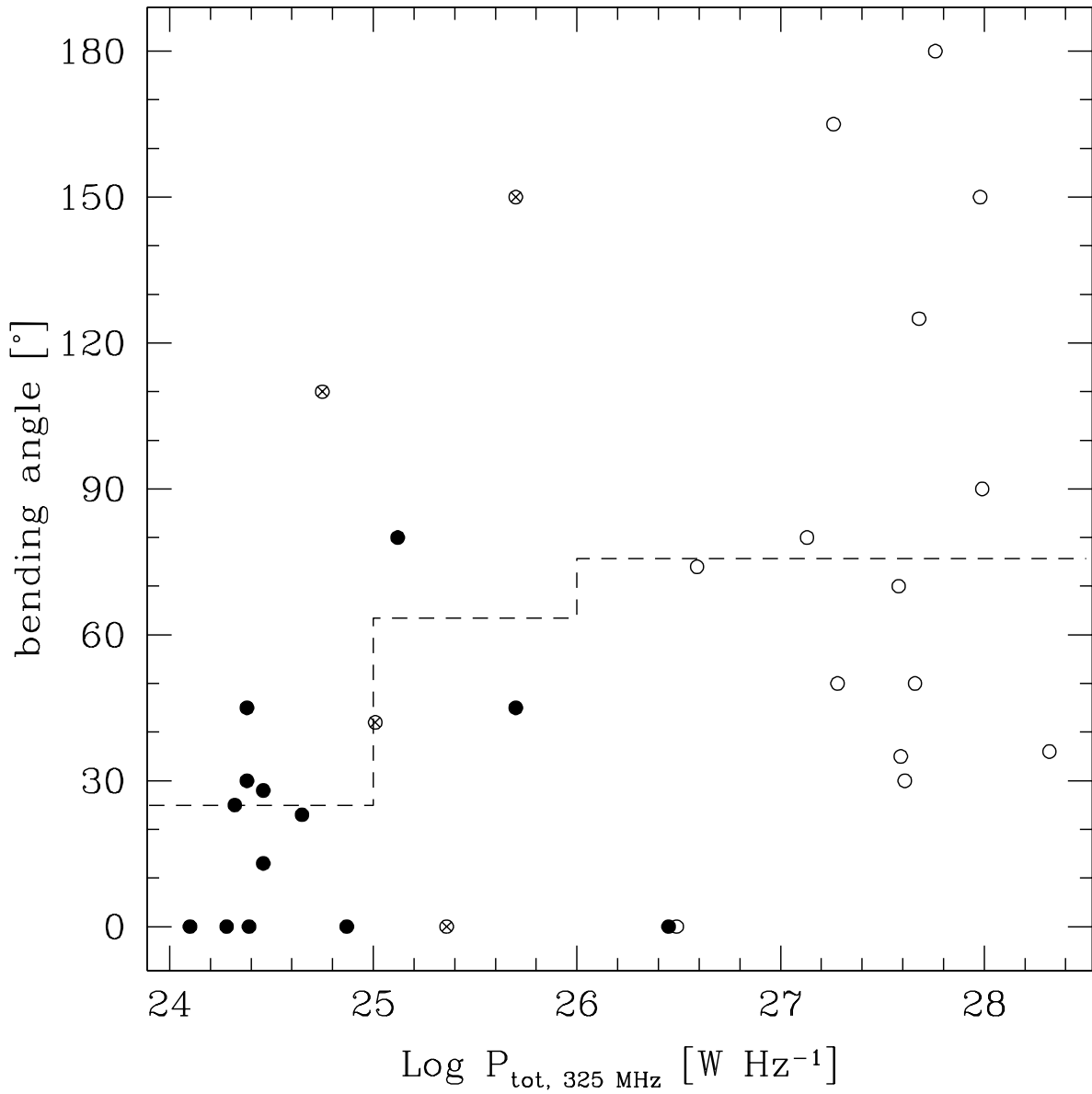


Fig. 11.— Bending angle vs. total radio power at low frequency (325 MHz). The diagram includes both BL Lacs from the present work (filled symbols) and the 1 Jy sample (empty symbols); the crossed symbols are the four objects common to both samples (1418+546, 1514–241, 1652+398, and 1807+698); the dashed line corresponds to the average bending angle in the three luminosity bins: $24 < \log P < 25$, $25 < \log P < 26$, and $\log P > 26$.

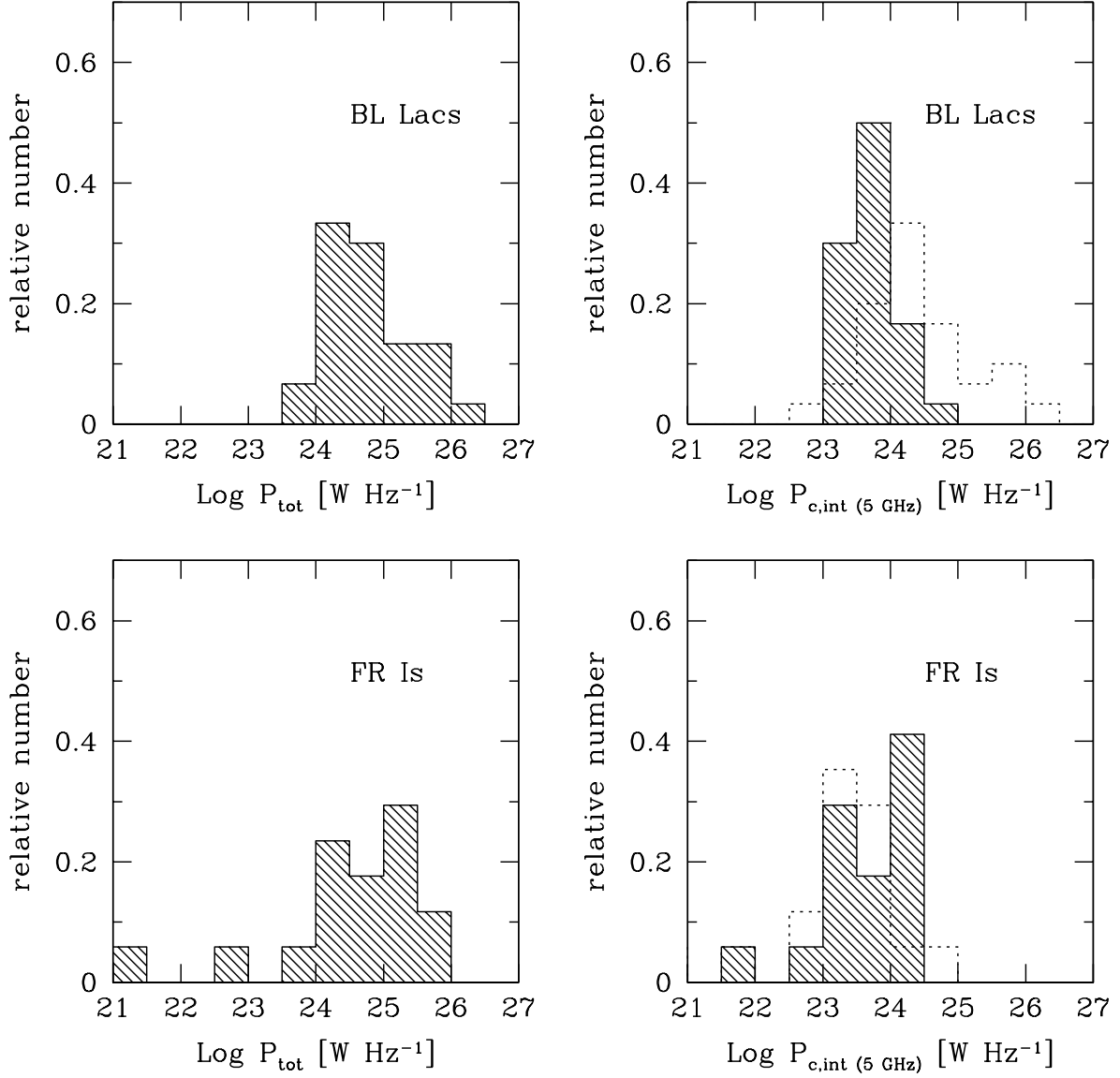


Fig. 12.— Distribution of total and intrinsic core power for objects in the present sample and FRI and LPC radio galaxies in a sample of radio galaxies (Giovannini et al. 2001). The dashed histograms overlayed to the intrinsic core power show the distribution of the observed values.